Distribution Agreement

In presenting this thesis as a partial fulfillment of the requirements for a degree from Emory University, I hereby grant to Emory University and its agents the non-exclusive license to archive, make accessible, and display my thesis in whole or in part in all forms of media, now or hereafter now, including display on the World Wide Web. I understand that I may select some access restrictions as part of the online submission of this thesis. I retain all ownership rights to the copyright of the thesis. I also retain the right to use in future works (such as articles or books) all or part of this thesis.

Gavin C. Touponse April 1, 2019

The Design and Assembly of 1D and 2D Multicomponent Collagen Mimetic Peptide Systems

by

Gavin C. Touponse

Dr. Vincent Conticello
Adviser

Department of Chemistry

Dr. Vincent Conticello

Adviser

Dr. Patrick Cafferty

Committee Member

Dr. Jose Soria

Committee Member

2019

The Design and Assembly of 1D and 2D Multicomponent Collagen Mimetic Peptide Systems

By

Gavin C. Touponse

Dr. Vincent Conticello

Adviser

An abstract of
a thesis submitted to the Faculty of Emory College of Arts and Sciences
of Emory University in partial fulfillment
of the requirements of the degree of
Bachelor of Sciences with Honors

Department of Chemistry

2019

Abstract

The Design and Assembly of 1D and 2D Multicomponent Collagen Mimetic Peptide Systems
By Gavin C. Touponse

The design of 1D and 2D multicomponent “soft” materials offers significant advantages over their single component counterparts. Multicomponent systems represent a viable option for introducing greater functionality and control over their assembled structures. However, fabrication methods for constructing multicomponent assemblies remains a significant challenge. Herein, we report the design of a series of collagen mimetic peptides (CMPs) that assemble into multicomponent ultra-large 1D tubes, having macroporous porosity, and 2D nanosheets. These assemblies comprise two or more peptides assembled via complementary electrostatic forces. We characterize their assembly using a suite of techniques including circular dichroism (CD) spectropolarimetry, transmission electron microscopy (TEM), dynamic light scattering (DLS), and atomic force microscopy (AFM). We demonstrate that by tuning the CMP sequences, we can tailor their assembly morphology and physical properties. Furthermore, we show that we can interconvert between 1D and 2D structures through pH changes of the assembly medium. These assemblies and, in particular, the 1D collagen tubes, represent an intriguing new addition into the biomolecular materials catalogue. The large physical dimensions of the tubes (pore size >100 nm) distinguishes these assemblies from other biomolecular 1D assemblies reported in literature. We envision that these assemblies may encapsulate large proteins or other biologically relevant molecules for applications in chemical sensing, catalysis, and as structural scaffolds for organizing nano- and mesoscale components. Altogether, these initial studies provide foundational design rules for assembling macroporous peptide-based tubes and nanosheets from multiple building blocks assembled through complementary coulombic interaction.

The Design and Assembly of 1D and 2D Multicomponent Collagen Mimetic Peptide Systems

By

Gavin C. Touponse

Dr. Vincent Conticello

Adviser

A thesis submitted to the Faculty of Emory College of Arts and Sciences
of Emory University in partial fulfillment
of the requirements of the degree of
Bachelor of Sciences with Honors

Department of Chemistry

2019

Acknowledgements

I would like to acknowledge Dr. Conticello for allowing me to join his research group and supporting me in my development as a chemistry student and researcher. I feel that without my experience in Dr. Conticello's lab, my chemistry education at Emory would be incomplete and far less meaningful.

I also owe much gratitude to fellow group member, Dr. Andrea Merg, who spent countless hours training me and providing his insights into my research project. Without Dr. Merg, the work presented in this thesis would not have been completed. Other group members who I would like to acknowledge include Dr. Charles Modlin, Spencer Hughes and Abraham Tuachi. Thank you all for your support and patience with me while working in the lab.

Finally, I would like to acknowledge Prof. Tianquan Lian for allowing us to use his atomic force microscope, Prof. Jen Heemstra for allowing us to use her lyophilizer, Prof. Brian Dyer for allowing us to use his dynamic light scattering instrument, and Prof. Khalid Saliata for his collaboration in obtaining fluorescent microscopy data.

Table of Contents

Introduction……1

Materials and Methods……..12

Materials……12

Peptide Synthesis/Purification……...12

Circular Dichroism……13

Transmission Electron Microscopy……...14

Zeta Potential Measurements……14

Atomic Force Microscopy……15

Stochastic Optical Reconstruction Microscopy……15

Results and Discussion……..16

Conclusion……34

Supporting Information……..37

References……..42

List of Figures

Figure 1. (A) Zika virus cryo-EM structure.[4] (B) Dynein cryogenic electron tomography structure.[5] (C) Depiction of the organization of the electron transport chain.[6]……...3

Figure 2. (A) Giant double-walled peptide nanotube of a β-sheet forming peptide.[10] (B) Cryo-EM structures of computationally designed 1D helical filaments adapted from Shen *et al.* [11]…...4

Figure 3. (A) Ultra-thin 2D peptoid nanosheets reported by Nam *et al.*[13] (B) Core-shell designed structures from block copolymers adapted from He *et al.*[14]…….……...6

Figure 4. (A) Responsive single-walled peptoid nanotubes.[16] (B) Superstructured responsive peptide-DNA networks reported by Freeman *et al*.[17]…..…….7

Figure 5. (A) TEM image, (B) SAXS spectrum, (C) electron diffraction image, (D) AFM topography and (E) tetragonal packed collagen helices model for NSI reported by Jiang *et al.*[20]..9

Figure 6. (A) CMP peptide sequences and (B) corresponding TEM adapted from Parmar *et al.*[25] ……10

Figure 7. (A) General formula for the peptide sequence of previously reported CMPs (blue; positively charged residues and triads, red; negatively charged residues and triads). Letter *n* indicates the number of canonical collagen triads whereas letters *m* and *p* indicate the number of positively and negatively charged triads, respectively. (B) Amino acid sequences of developed CMPs: **R4P6** and **P6E4**. (C) Proposed assembly schematic for multicomponent 2D peptide nanosheets comprised of peptides **R4P6** and **P6E4**……..11

Figure 8. (A) CD spectra of peptides **R4P6** and **P6E4** (1 mg/mL) in 20 mM MOPS buffer, pH 7. (B) First derivative plot of the CD signal at 224 nm as a function of increasing temperature for **R4P6** and **P6E4** (0.5 mg/mL). (C) RPN values at the time points of 1 hour, 24 hours, 3 days and 7……..17

Figure 9. (A) TEM image of a single representative collagen tube constructed from **R4P6** and **P6E4**. (B) TEM image of a polydisperse group of collagen structures…….18

Figure 10. (A) Enlarged image of a **R4P6/P6E4** tube for visualization of distinct layering. Inset scale bar is equal to 20 nm. (B) Histogram of outer diameter (blue) and inner diameter (red) for **R4P6/P6E4** tubes. A Gaussian distribution was fitted to each of the histograms with the average and standard deviation displayed above plot (N = 56)……..19

Figure 11. (A) AFM tapping mode topography image of **R4P6/P6E4** peptide tubes. Inset scale bar is equal to 500 nm. (B) AFM tapping mode amplitude image. (C) Line trace depicting the height of the tube indicated in the inset of (A)……..20

Figure 12. (A) Modified assembly schematic for the formation of multicomponent 1D macroporous tubes…….21

Figure 13. (A) Peptide sequence for **CP 262**. (B) Proposed assembly schematic for **CP 262** 2D peptide sheets. ……..….22

Figure 14. (A) CD spectrum of peptide **CP 262** (1 mg/mL) in 20 mM TAPS buffer, pH 8. (B) First derivative plot of CD signal at 224 nm as a function of increasing temperature for **CP 262** (0.5 mg/mL) in 20 mM TAPS, pH 8. ……...……...….23

Figure 15. (A) Single representative **CP 262** 2D peptide nanosheet. (B) Many polydisperse **CP 262** 2D peptide nanosheets...…….... …….23

Figure 16. (A) CD spectrum of peptide **R6P6** (1 mg/mL) in 20 mM MOPS buffer, pH 7. (B) First derivative plot of CD signal at 224 nm as a function of increasing temperature for **R6P6** (0.5 mg/mL) in 20 mM MES pH 6, MOPS pH 7, and TAPS pH 8. (C) RPN values at the time points of 1 hour, 24 hours, 3 days and 7 days…….24

Figure 17. (A) 2D large **R6P6**/**P6E4** peptide sheets formed at pH 7 (similar to pH 6 structures). (B) Low magnification image of pH 8 **R6P6/P6E4** peptide tubes and (C) high magnification

image of a **R4P6/P6E4** tube for visualization of distinct layering. Inset scale bar is equal to 20 nm. (D) Histogram of outer diameter (blue) and inner diameter (red) for **R6P6/P6E4** tubes. A Gaussian distribution was fitted to each of the histograms with the average and standard deviation displayed above plot (N = 61)……25

Figure 18. (A) AFM tapping mode topography image of **R6P6/P6E4** peptide tubes. Inset scale bar is equal to 500 nm. (B) AFM tapping mode amplitude image. (C) Line trace depicting the height of the tube indicated in the inset of (A). (D) AFM tapping mode topography image of **R6P6/P6E4** peptide sheets. (E) AFM tapping mode amplitude image. (F) Line trace depicting the height of the sheet across the dashed line in (A)……..27

Figure 19. (A) TEM image of doped (50% **R4P6** /50% **R6P6)/P6E4** single walled tubes. (B) Histogram of outer diameter (blue) of doped (50% **R4P6** /50% **R6P6)/P6E4** single walled tubes. A Gaussian distribution was fitted to the histogram with the average and standard deviation displayed above plot……..28

Figure 20. (A) Zeta potential measurements of aqueous buffered solutions of **R6P6** peptide nanosheets at pH 6 (MES, 20mM) and pH 7 (MOPS, 20 mM) as well as peptide tubes comprising **R4P6** (MOPS pH 7, 20mM) or **R6P6** (TAPS pH 8, 20mM). (B) Zeta potential dependence on the relative concentrations of **R6P6** and **R4P6** for doped tri-peptide assembly experiments all performed in pH 7 buffer (MOPS, 20mM)……..29

Figure 21. (A) Proposed interaction between anionic Au particles and (B) cationic Au particles with the peptide tubes. (C) TEM of anionic Au particle and (D) cationic particle interactions with the peptide tubes. (E) Proposed interaction between anionic Au particles and (F) cationic Au particles with the peptide nanosheets. (G) TEM of anionic Au particle and (H) cationic particle interactions with the peptide nanosheets.…….. ……30

Figure 22. (A) Proposed transition mechanism without and (B) with disassembly. (C) pH 6 structures titrated to pH 8 and (D) pH 8 structures titrated to pH 6 transforming from sheets to tubes and vice versa. ……...……..33

Figure 23. (A) Fluorescent microscopy image of pH 7 **R6P6/P6E4** 2D peptide nanosheets functionalized with biotin-streptavidin conjugated to Cy3B dye. (B) Fluorescent microscopy image of pH 8 **R6P6/P6E4** 1D peptide tube functionalized with biotin-streptavidin conjugated to Cy3B dye.…….……...……..34

Figure S1. HPLC trace for **R4P6**……..37

Figure S2. MALDI-TOF mass spectrum of the peptide, **R4P6,** after HPLC re-purification…...37

Figure S3. HPLC trace for **P6E4**……..37

Figure S4. MALDI-TOF mass spectrum of **P6E4** after HPLC re-purification……38

Figure S5. HPLC trace for **R6P6** (SynPep)……..38

Figure S6. MALDI-TOF mass spectrum of **R6P6** after dialysis……..38

Figure S7. HPLC trace for **CP 262**……...39

Figure S8. MALDI-TOF mass spectrum of **CP 262** after HPLC re-purification…….39

Figure S9. HPLC trace of **Biotin-R6P6**……...39

Figure S10. MALDI-TOF mass spectrum of **Biotin-R6P6** after HPLC re-purification……..40

Figure S11. (A) Control TEM of individual peptide **R4P6**, (B) **R6P6**, and (C) **P6E4**……40

Figure S12. (A) **Biotin-R6P6/P6E4** pH 7 peptide nanosheets and (B) **Biotin-R6P6/P6E4** pH 8 peptide tubes……..41

Introduction

As technology continues to rapidly grow, the need for developing new materials has risen across a variety of fields spanning from biotechnology to energy and electronics, to name a few. Developed recently, the field of materials science comprises many disciplines such as physics and engineering; however, chemistry remains perhaps the most essential portion of the field due to the need for characterization and manipulation of new materials at the molecular scale. It is through developing an increased understanding of the molecules and their interactions with one another that scientists have been able to make crucial advancements resulting in technologies such as biocompatible prosthetics, machines, delivery devices or other non-biological materials including integrate-circuit chips and increasingly efficient fuels.[1] While these materials developments are an integral part of our increasingly advanced society, the focus of this thesis will be on the development, characterization, and design of responsive multicomponent biological materials at the nano- and mesoscale.

Over millions of years, the natural world has evolved a diverse array of materials spanning from zero dimensions (0D) up to three dimensions (3D). Specifically, of key interest to this work are one dimensional (1D) and two dimensional (2D) materials within the size regime of 100 nm to 1 μm. Although the development of 2D materials at the given scale has progressed over the past decades, there is an apparent lack of 1D tubular structures that fall into this size range; these tubes are so-called “macroporous” and are defined as having a diameter greater than 50 nm.[2] In addition to reporting one of the first instances of a macroporous peptide tube, this report describes an important expansion to the materials catalogue through developing an additional class of peptides that mediate between the formation of 1D and 2D structures.[3] There are many examples in the literature of 1D and, to a lesser extent, 2D materials; however, we

propose that current systems are limited in their structural control due to their incorporation of only single components. In this work, we propose that the development of multicomponent self-assembling peptide systems serves as a general solution and design principle for allowing us to mediate between 1D and higher dimension systems as well as introducing an increased potential for chemical functionalization.

In looking for inspiration for the design of biocompatible materials, we often turn to nature, which has developed many complex structural and functional molecular assemblies. These assemblies have been observed to form astoundingly complex mechanical structures, vessels, and functional systems through the use of oligomers as building blocks constructed from simple monomers such as amino acids. Recently, cryogenic electron microscopy (cryo-EM) has allowed for researchers to solve biological structures such as Zika virus to near-atomic resolution.[4] An alternative example whose crystal structure was solved through X-ray crystallography, tobacco mosaic virus, has an entirely different rod-like structural morphology to encapsulate its RNA. Despite the complexity and function of these protein capsid structures, nature has evolved even more intricate systems that function as molecular machines in moving materials around cells through extensive microtubule networks, for example.[5] The complex protein, dynein, functions through the use of adenosine triphosphate (ATP) to move cellular contents towards the minus ends of microtubules and is crucial for many cellular processes such as mitosis. Lastly, cells have developed complex systems of proteins spatially oriented within membranes including the electron transport chain and photosystem I for harvesting energy from the environment.[6,7]

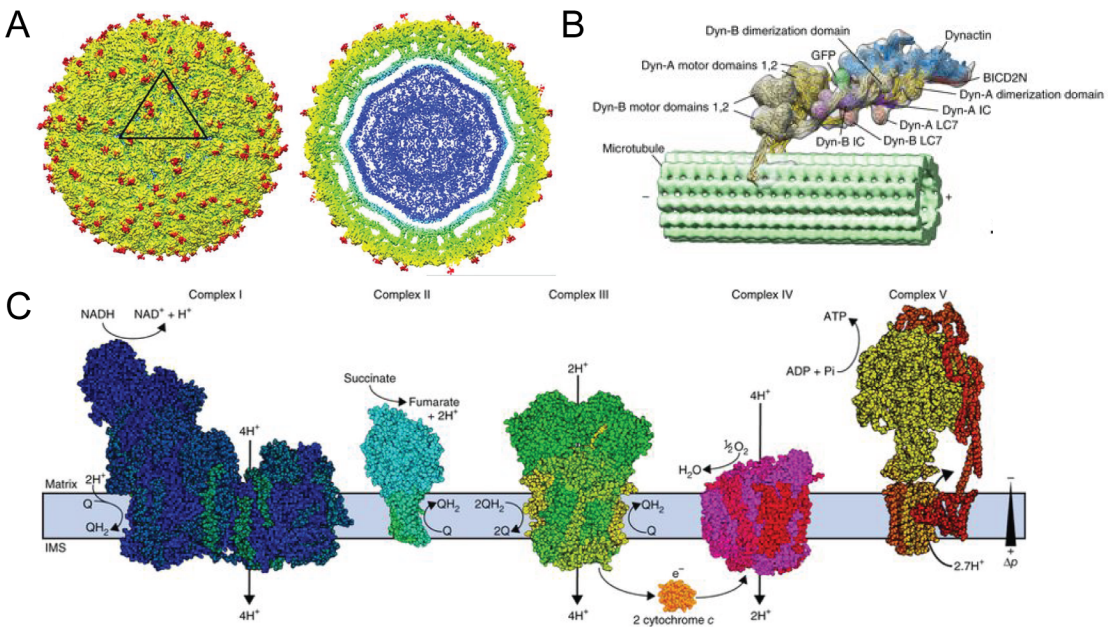

Figure 1. (A) Zika virus cryo-EM structure.[4] (B) Dynein cryogenic electron tomography structure.[5] (C) Depiction of the organization of the electron transport chain.[6]

Biomaterials science aims to examine structures from biology, such as those mentioned above, to determine the principles that organisms use to form these intricate and highly functional systems so that the principles can be used for the design of new, synthetic, biomaterials. Possible functions for such biomaterials include structural encapsulation, selective membranes, bottom-up templates or delivery of small molecules, enzymes, and genetic information. However, before novel structures can developed for potential use, principles of self-assembly must be understood through computation, experiment and characterization of simple and complex structures such as vesicles, bilayers, liposomes, nanosheets, nanotubes and protein complexes in order to create tailorable structures of specified sizes and shapes. Soft materials development aims to use the diverse array of natural and non-natural biomolecules engineered to create materials compatible with those seen in biology through processes of self-assembly in the bottom-up design of materials to carry out functions in biological systems.[8]

While there are many examples of 1D tubular structures in nature, scientists did not begin to construct these materials until quite recently where they have found that peptide oligomers are ideal candidates for assembly into materials because of their biocompatibility, highly complex assembly behavior, and extensive chemical diversity. In an early example of the creation of biocompatible nanotubes, Ghadiri *et al.* describe the creation of peptide nanotubes comprising of alternating D- and L- cyclic peptoid molecules that assembled into tubes on the scale of 1.5 nm in diameter.[9] More recently, through exploring the amyloid Aβ peptide family, Jin and coworkers developed so-called "giant" double-walled peptide nanotubes that assembled on the scale of ~10 nm, which are almost an order of magnitude larger than the cyclic peptide tubes reported by Ghadiri *et al*.[10] Work done by Chen and co-workers also represents an single example of many where a β-sheet forming peptide assembles into 1D fibers. The type of hydrogen bonding involved serves as the driving force behind the majority of 1D filamentous self-assembly.[11]

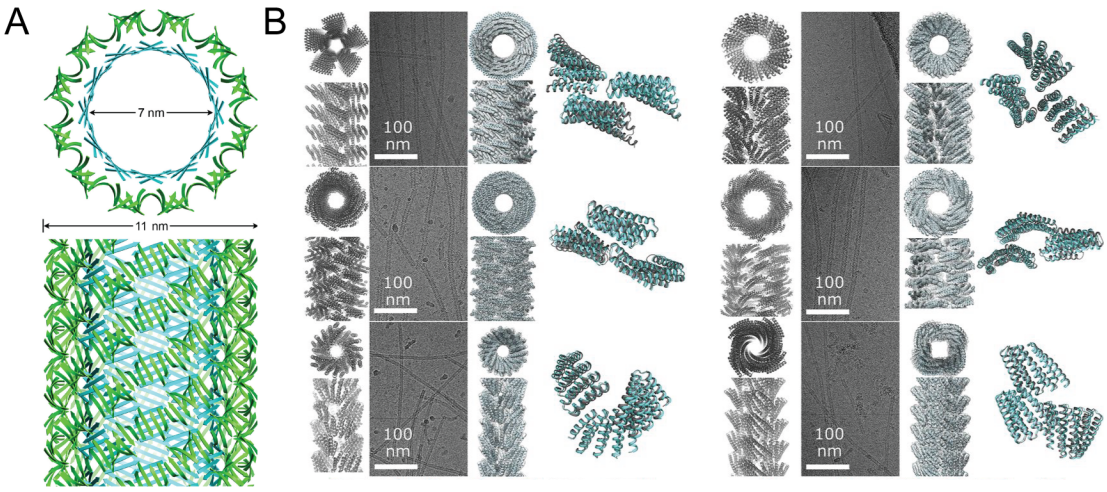

Figure 2. (A) Giant double-walled peptide nanotube of a β-sheet forming peptide.[10] (B) Cryo-EM structures of computationally designed 1D helical filaments adapted from Shen *et al.* [11]

Alternative methods of development have emerged to include helical filaments in addition to β-sheet forming peptides. Shen *et al.* reported the computational design of six different monomeric alpha helical peptides that form filaments with defined structural properties.[12] Systematic manipulation of the designed fibers was achieved through the use of computational modeling. Such modeling represents an alternative method to rational design in the creation of self-assembling materials. These computational models illustrate how using Angstrom scale interactions can be computationally manipulated to exert control on the micrometer scale with the resulting structures being fully characterized to near-atomic resolution through the use of cryo-EM. Despite the significance of the examples mentioned, all pertain to tubular structures on the scale of 1-10 nm (*ie.* nanoscale). While the published research represents significant advances, it also illustrates the lack of construction of macroporous peptide tubes which serve as the foundation of this reported work.

Provided that a central tenant of this reported work is to describe how the creation of multicomponent peptide systems can serve general design principle to mediate between the formation of 1D and 2D structures, it becomes relevant to discuss recent developments in 2D peptide structures. Less progress has been made in developing 2D materials due to difficultly in preventing association of the materials into 1D and 3D structures.[1] However, due to their unique property of having intrinsically high surface area resulting from their planar geometry, 2D materials are of great interest. Recent developments in creating ultra-thin planar structures include work published by Zuckermann and co-workers who reported the creation of peptoid nanosheets.[13] The nanosheets were created through complementary charge interactions between two peptoid polymers, which are non-natural protein mimicking molecules.

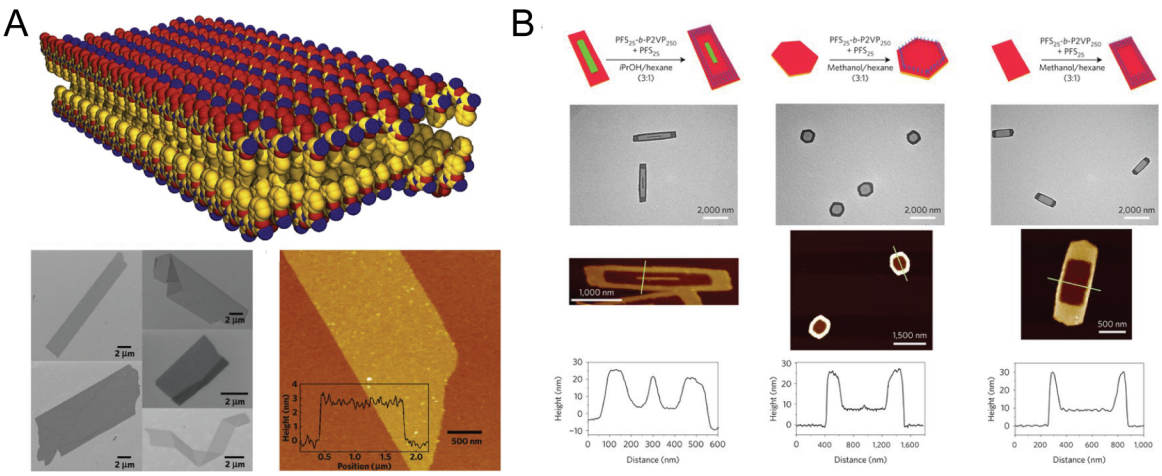

Figure 3. (A) Ultra-thin 2D peptoid nanosheets reported by Nam *et al.*[13] (B) Core-shell designed structures from block copolymers adapted from He *et al.*[14]

Furthermore, researchers have progressed to develop more complex multicomponent 2D materials through an array of techniques. In one such example, Ian Manners has focused on a seeded-growth approach using multiple block copolymers to demonstrated the construction of multicomponent 2D materials with mesoscale control of size, shape and, most significantly, patterning across the template surface.[14,15] These core-shell structures demonstrate an alternative method for the incorporation of a multicomponent system to introduce an added level of complexity to a self-assembled structure. These core-shell constructed 2D assemblies contain an uneven distribution of components whereas the system reported herein assembles in a proposed homogeneous fashion where components are evenly distributed throughout the material. The use of these methods has consequences on the potential functionality of the final materials.

Although there have been advances in developing a variety of peptide nanoscale tubes through rational and computational design, the development of materials that exhibit response to external stimuli remains a challenge.[16] As we know, biological systems rely on the ability to respond to a diverse array of stimuli which we must also consider in designing synthetic

replacements for these biological structures. Jin *et al.* developed a series of sequence-defined peptoids that exhibit structural control via sequence manipulation, similar to those examples previously mentioned, but, in addition, undergo pH triggered reversible contraction-expansion motion to alter the tube diameter.[16]

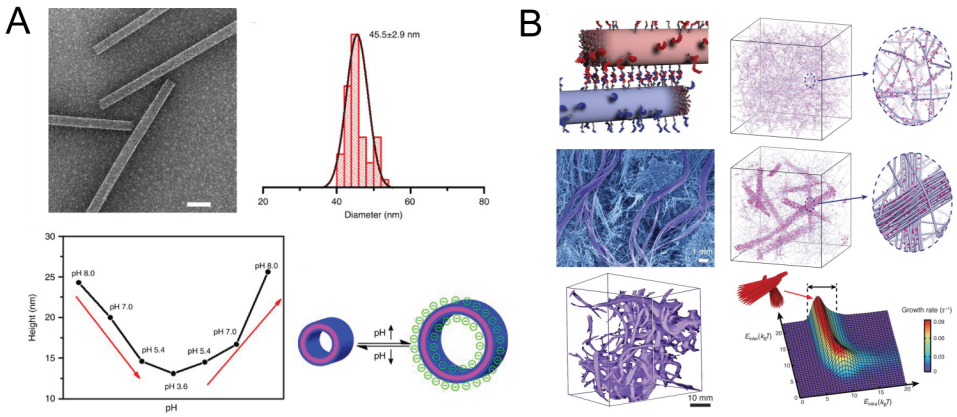

Figure 4. (A) Responsive single-walled peptoid nanotubes.[16] (B) Superstructured responsive peptide-DNA networks reported by Freeman *et al.*[17]

Responsive systems have been created on larger scales as well. Stupp and co-workers reported the development of peptide-DNA conjugates that could reversibly assemble into super-structured networks of intertwined fibers.[17] While the development of 1D and 2D assemblies represents a worthwhile challenge, implementation into biological systems may also require responsive tunability that must be incorporated into materials during their developmental phase.

For decades, collagen has been an intense area of research in the realm of biomaterials due to it being the most prevalent fibrous protein in the animal kingdom comprising 25-35% of all protein in the human body. Collagen exists primarily in the extracellular matrix and is an essential component of connective tissue where it forms tough fibers that provide resistance to tensile and compressive forces.[18] Generally, native collagen exists in Type I, II, or III, but

regardless of type, collagen can be characterized by its repeat triad sequence Xaa – Yaa – Gly. In the canonical collagen pro-triple helix forming triad, Proline (Pro) and (4R)-hydroxyproline (Hyp) occupy the Xaa and Yaa positions, respectively. The repeat triad sequence of collagen allows for folding into a unique triple helix conformation that requires a high imino acid content in the sequences of the individual strands. Due to its prevalence, collagen has been the subject of much research. In 2007, a collagen based mimetic peptide (CMP) called **CPII** demonstrated controlled self-assembly into 1D fibers and was also observed to form into defined 2D nanoscale sheets under certain conditions.[19] This discovery resulted in an additional project in constructing 2D materials from CMPs.

Reported peptides containing non-canonical imino acid, aminoproline, **NSI** and **NSIII** displayed the propensity to self-assemble into structurally defined nanoscale peptide sheets through complementary charged interactions.[20,21] Characterization of the reported structures allowed for the creation of a model where adjacent collagen triple helices pack in an antiparallel fashion into a tetragonal geometry crystalline lattice.

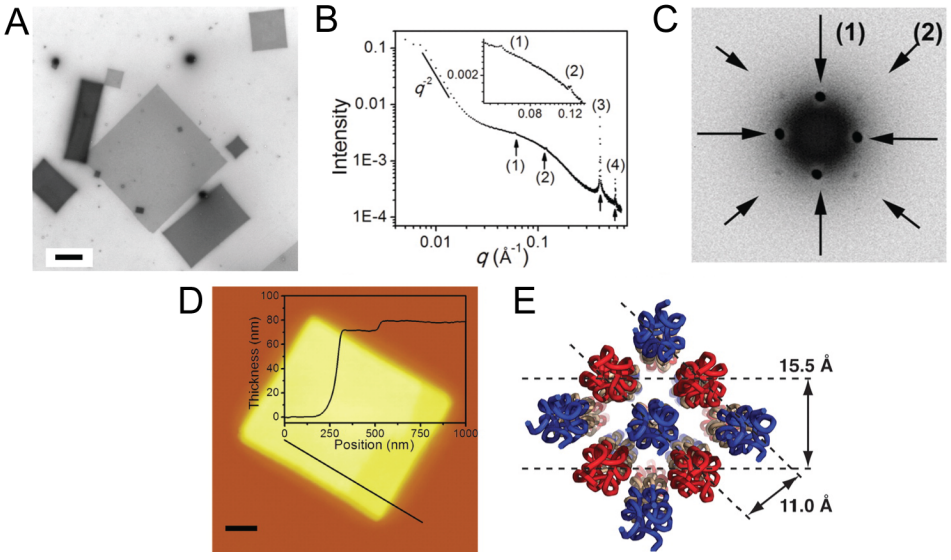

Figure 5. (A) TEM image, (B) SAXS spectrum, (C) electron diffraction image, (D) AFM topography and (E) tetragonal packed collagen helices model for **NSI** reported by Jiang *et al.*[20]

Further research was conducted to expand the amount of versatility of the structures. One project, involved the construction of peptide sequences with extended charged triads at either the N-terminus or the C-terminus, which were designed to contain positive and negative charge groups, respectively.[22] These peptides were designed to contain charged surfaces, which would allow for the controlled growth of the sheets in the z-direction through complementary interaction between sheets with positive and negative surface charge. Consistent with the hypothesis, stacked sheets were observed via TEM and confirmed through AFM analysis. This work demonstrates design principles regarding the manipulation of charged blocks in CMPs as another way to control the assembly of collagen into higher order structures. These principles are employed similarly in the construction of multicomponent collagen peptide systems.

Despite advances in the development of single peptide-based systems, these materials are limited in their functional potential due to their composition.[23] As demonstrated previously, the N-terminus serves as a viable site to functionalize peptide systems through biotin,[24] for example; however, incorporation of single peptides into structures limits the functional potential to one possible linkage. To overcome such limitations, Parmar *et al*. described the assembly of multicomponent CMP systems into fibers and large 2D peptide nanosheets.[25] The reported structures represent one of the few instances of a multicomponent self-assembling 2D CMP peptide system.

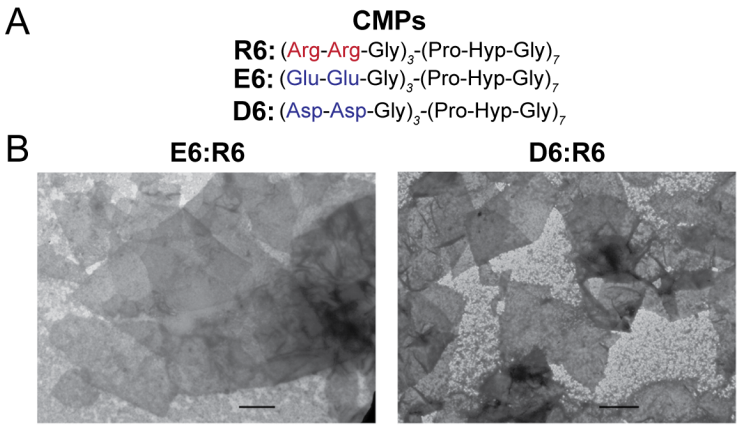

Figure 6. (A) CMP peptide sequences and (B) corresponding TEM adapted from Parmar *et al.*[25]

The structures shown in Figure 6 were poorly defined and were not fully characterized beyond methods of circular dichroism, transmission electron microscopy and DLS. In contrast to previous success with self-assembling CMPs, which all utilized sequences designed to pack in an antiparallel fashion, Parmar *et al.* designed multiple peptides to pack in parallel. Based on these collagen assemblies, we hypothesized that the development of a multicomponent CMP system designed to pack antiparallel would lead to more favorable coulombic interactions between helices therefore promoting the formation of more well-defined and structurally homogeneous structures for further characterization. Moreover, our hypothesis led to the design of asymmetric peptide sequences observed to assemble into mesoscale 1D collagen tubes, 2D collagen nanosheets and exhibit pH responsiveness transitioning between 1D and 2D morphologies.

Here, we report the preparation of a family of CMPs of varying length and amino acid content designed to assemble into well-defined 1D and 2D structures. We demonstrate that through manipulation of peptide sequence and experimental conditions, we can mediate a transition between 1D and 2D assembly morphology, which has not previously been demonstrated for a multicomponent peptide system comprised of CMPs and furthermore, we

demonstrate the functional potential of these collagen-based materials. Before proceeding, we introduce the general formula for reported CMPs and initial peptide sequences that we have termed **R4P6** and **P6E4** (Figure 7A-B).

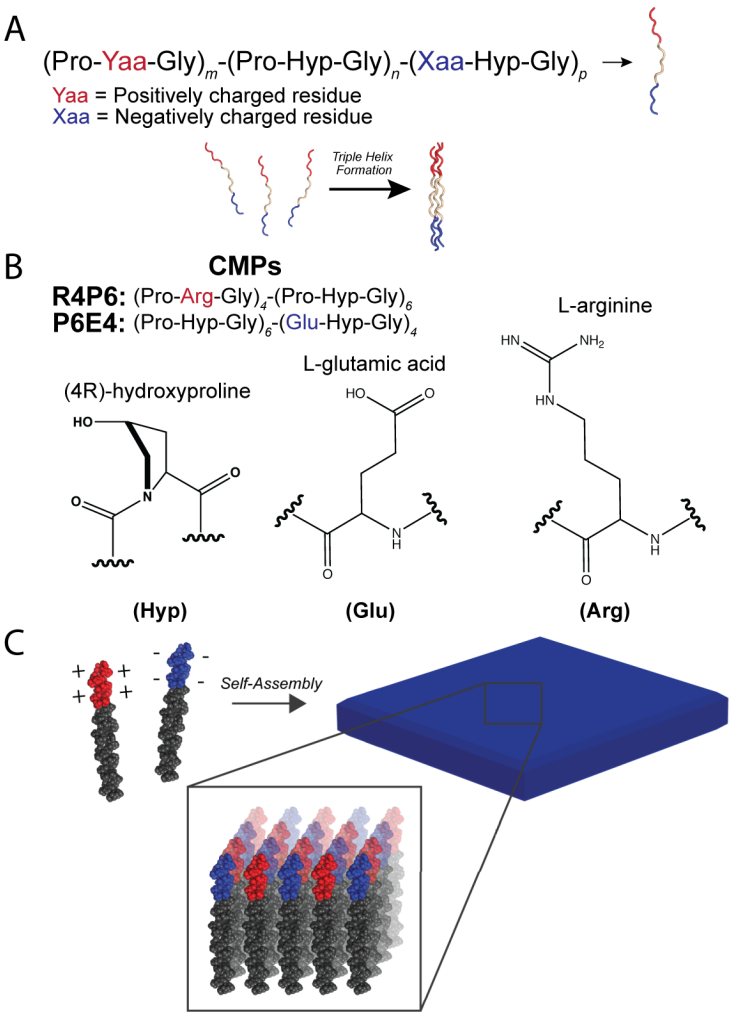

Figure 7. (A) General formula for the peptide sequence of previously reported CMPs (blue; positively charged residues and triads, red; negatively charged residues and triads). Letter *n* indicates the number of canonical collagen triads whereas letters *m* and *p* indicate the number of positively and negatively charged triads, respectively. (B) Amino acid sequences of developed CMPs: **R4P6** and **P6E4**. (C) Proposed assembly schematic for multicomponent 2D peptide nanosheets comprised of peptides **R4P6** and **P6E4**.

The materials reported utilize the structural motif of the collagen triple helix, acting as a rigid rod, to expand the assembly space in the literature for 1D and 2D "soft" materials through a bottom-up assembly process. Additionally, the reported structures possess unique properties in size that lead to the hypothesis that they have superior mechanical properties to similar structures reported previously in the literature. Lastly, this work adds another pH responsive system to the materials catalog. These materials possess a high potential for further development and incorporation into artificial biological tissues, delivery vehicles, sensory devices, and reaction vessels.

Materials and Methods

Materials. Unless otherwise stated, all chemical reagents used were purchased from Sigma-Aldrich Chemical Co. (St. Louis, MO), or Anaspec, Inc. (Fremont, CA). Chemicals were used as purchased with no further purification. The following peptides were purchased from SynPep Corporation (Dublin, CA): **R6P6**.

Peptide Synthesis and Purification. A CEM Liberty microwave-assisted peptide synthesizer was employed to make the following peptides: **R4P6, Biotin-R6P6, P6E4, and CP 262.** Standard Fmoc protection chemistry was used with Fmoc-Gly-HMP-TentaGel resin. HBTU and DIEA were employed as the activator and activator base, respectively, with deprotection of Fmoc groups through the use of 20% piperidine in DMF. Crude peptide products were subjected to cleavage from the support resin through standard protocol consisting of 92.5% TFA, 2.5% TIS, 2.5% DODT, and 2.5% water (TFA: trifluoroacetic acid, DODT: 3,6-Dioxa-1,8-octane-dithiol, TIS: Triisopropylsilane). Peptides were precipitated from solution through centrifugation

at 4ºC after mixing with cold Et_2O. A Shimadzu LC-20AP preparatory scale reverse-phase HPLC with a C18 column was used to purify and re-purify peptides (SI Figures 1, 3, 7, 9). A linear gradient of water-acetonitrile was used with 0.1% TFA. After collection of desired products, samples were assessed using matrix-assisted laser desorption/ionization time of flight (MALDI-TOF) mass spectrometry with CHCA matrix (CHCA: α-Cyano-4-hydroxycinnamic acid, SI Figures 2, 4, 6, 8, 10). Peptides were dialyzed against pure HPLC grade water to remove remaining TFA in 2,000 Da dialysis containers obtained from ThermoFisher Scientific (Waltham, MA), lyophilized, and stored at -20ºC. Known amounts of peptide were weighed using an analytical balance and dissolved in water before being separated into known amounts, lyophilized and stored at -20ºC prior to assembly. For assembly, peptides were dissolved using MES, MOPS, and TAPS (20mM pH 6, pH 7, and pH 8, respectively) at appropriate concentrations. All samples were annealed from 90ºC to 4ºC or 90ºC to 25ºC at a gradient of 0.2ºC/min and stored at 4ºC or room temperature. Arginine containing peptides were annealed first using an annealing protocol from 90ºC to 4ºC and allowed to sit for at least one week. Next, glutamic acid peptide, **P6E4**, was annealed 90ºC to 25ºC and added to an arginine containing peptide that had recently been warmed to room temperature. The peptide mixtures were then allowed to incubate at room temperature before characterization.

Circular Dichroism. CD measurements were obtained using a Jasco J-810 or J-1500 spectropolarimeter. Samples were injected into a 0.1 mm quartz cell for CD spectra or a 1 mm quartz cuvette for CD melting curves. Background spectra were obtained using the appropriate buffer for each sample and subtracted from the spectrum prior to graphing. Spectra were collected from 260 nm to 190 nm using a scanning speed of 100 nm/min, bandwidth of 2 nm, data pitch of 0.1 nm and a D.I.T. of 4 seconds at specified temperatures. Melting curves were

obtained through monitoring the CD signal at 224 nm from 5ºC to 85ºC using a temperature gradient of 20ºC/hour. T_m was estimated by calculating the minimum of the first derivative of the temperature vs. CD (mdeg) melting curve.

Transmission Electron Microscopy. TEM imaging was conducted using a Hitachi H-7500 microscope at an accelerating voltage of 80 kV. Unless otherwise noted, peptide assemblies were placed on 200-mesh carbon coated copper grids obtained from Electron Microscopy Sciences (Hatfield, PA) and incubated with 1% uranyl acetate stain before being wicked away with filter paper and allowing the grid to dry. Dimensions of assembled structures were assessed through the use of ImageJ.

Gold nanoparticle assays were conducted through a repeated process of centrifugation until a pellet of assembly was observed, removal of the supernatant and resuspension in clean buffer. Cationic amine functionalized gold nanoparticles 15 nm in size and anionic carboxylic acid functionalized gold particles 15 nm in size were purchased from Nanocs (New York, NY). 15µL of undiluted particles were added to assemblies and allowed to incubate for 30 min to 1 hour on the laboratory bench at room temperature before centrifugation and resuspension. TEM grids were prepared as stated above and washed once with 5µL of HPLC grade water.

Titration experiments were conducted through adding small aliquots of 0.05M NaOH and 0.05M HCl while monitoring with a pH meter.

Zeta Potential Measurements. A Particulate Systems NanoPlus 3 instrument was used to obtain zeta potential measurements. The NanoPlus 3 obtains zeta potential data through use of the electrophoretic light scattering technique based on the Doppler Effect. All measurements were obtained on 0.2 mg/mL solutions of assembled structures in aqueous buffer solution with MES, MOPS, or TAPS (20 mM, pH 6.0, 7.0, or 8.0, respectively). Samples were diluted at room

temperature immediately prior to data collection. Multiple measurements were obtained and used to calculate standard deviation, which is represented with error bars.

Atomic Force Microscopy. An Asylum MFP-3D atomic force microscope was used to collect AFM images using tapping mode. Ultrasharp AFM tips with a resonance frequency of 150 Hz and a force constant of 5 N/m (Budget Sensors, SHR-150, Wetzlar, Germany) were employed for the data collection. A scanning rate of 1 Hz was used. All AFM images were obtained from samples prepared on carbon coated copper 200 mesh TEM grids, as described above, after appropriate washing with HPLC water.

Stochastic Optical Reconstruction Microscopy (STORM). A No. 1.5 glass slide with dimensions 25 × 75 mm was cleaned for 15 minutes by sonication in MilliQ (18.2 MΩ cm^{-}) water. The sample was then sonicated for 15 minutes in pure ethanol and dried under a stream of nitrogen gas. The silicon glass was etched by piranha solution (v/v = 3:7 hydrogen peroxide/sulfuric acid) for 30 minutes. The cleaned substrates were rinsed repeatedly with MilliQ water, washed with ethanol, and oven dried. A home-made Delrin microfluidic chamber was attached to the slide and 50 μL of sample was added for imaging. The fluorescent microscope was equipped with a Nikon Intensilight epifluorescence source and CFI Apo 100 × NA 1.49 objective lens (Toyko, Japan). All of the reported experiments were performed using the TRITC filter cube (tetramethylrhodamine isothiocyanate) and reflection interference contrast microscopy (RICM) cube set supplied by Chroma (Bellows Falls, VT). Biotinylated peptide samples were mixed with a small aliquot of 0.3 mg/mL streptavidin-Cy3B and incubated for 1 hour before imaging.

Results and Discussion

To test our central hypothesis that an antiparallel packing multicomponent system would assemble into well-defined structures, two new CMP sequences, **R4P6** and **P6E4,** were designed and synthesized (Figure 7B). Similar to previous work reported with multicomponent CMPs,[25] both **R4P6** and **P6E4** contain asymmetric charge distributions across the length of the peptides. Positively charged triads incorporated the natural amino acid, Arginine (Arg), in the Yaa position creating (Pro-Arg-Gly) triads at the N-terminus of **R4P6** while negatively charged triads at the C-terminus of **P6E4** utilized Glutamic Acid (Glu) in the Xaa position resulting in (Glu-Hyp-Gly) triads. Both peptides contained six canonical pro-triple helix (Pro-Hyp-Gly) triads. Positive and negative residue identity and position were chosen based on prior host—guest studies of collagen-based peptide systems.[26] The respective residues and positions were the most stable collagen substitutions.

Initial characterization of the two peptides included circular dichroism (CD) spectropolarimetry studies in order to understand the propensity of **R4P6** and **E4P6** for forming triple helical conformation in aqueous buffered solution. A characteristic CD spectrum of the collagen triple helix consists of a maximum peak at 224 nm and a minimum peak at 198 nm. The ratio of the positive peak to the negative peak, termed the RPN value, serves as an indicator of a given peptides propensity for forming a triple helix conformation. An RPN value of ≥0.10 is consistent with a stable triple helix.

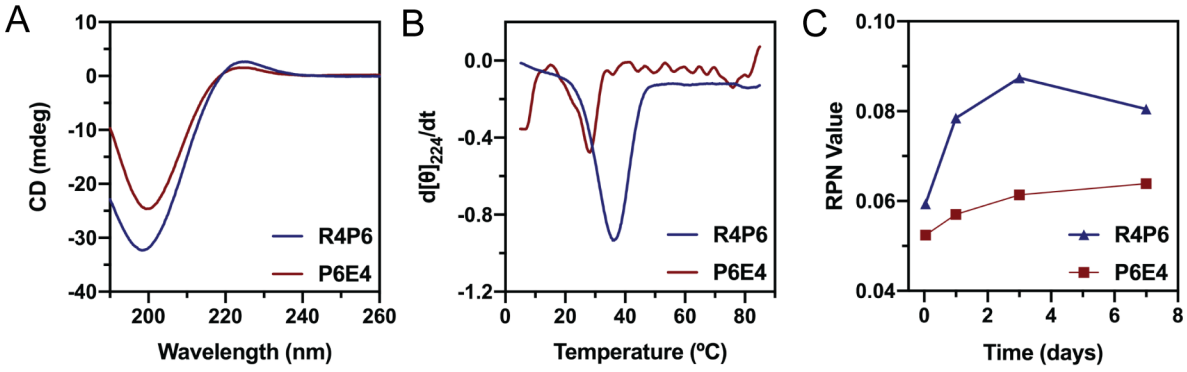

Figure 8. (A) CD spectra of peptides **R4P6** and **P6E4** (1 mg/mL) in 20 mM MOPS buffer, pH 7. (B) First derivative plot of the CD signal at 224 nm as a function of increasing temperature for **R4P6** and **P6E4** (0.5 mg/mL). (C) RPN values at the time points of 1 hour, 24 hours, 3 days and 7.

As depicted in Figure 8, **R4P6** and **P6E4** displayed propensity for forming relatively stable triple helices with RPN values of 0.08 and 0.06, respectively, after incubation for one week at 4ºC. RPN values of less than 0.10 can be rationalized on the basis that charged residues at the termini generate unfavorable repulsive forces. In addition to assessing relative helix stability, time studies monitoring the RPN values were utilized to assess the rate of triple helix formation over 1 week (Figure 8C). **P6E4** exhibited a slower rate of formation as observed by the slower increase in RPN value compared to **R4P6**. The lower RPN values of **P6E4** are also indicative of decreased triple helix stability. From these studies, **P6E4** was chosen as the rate limiting peptide for all assembly experiments based on the hypothesis that the less stable peptide would contribute to controlling the rate of assembly formation; however, this hypothesis was not further investigated due to the success of the assembly experiments.

Thermal denaturation studies were employed to study the relative stabilities of each of the two peptides of interest. The melting temperature (T_m) was calculated by taking the minimum of the first derivative of the melting curve. In addition to displaying a higher rate of triple helical formation, **R4P6** displayed a higher T_m at 37ºC indicating a higher relative stability when compared with **P6E4** (T_m = 28ºC). It has been hypothesized in the literature that Arg forms favorable interhelical and intrahelical hydrogen bonds when replacing Hyp in the canonical collagen sequence therefore having significantly less of a destabilizing effect on the formation of

the triple helix when compared to other amino acid residues.[26] Comparatively, although Glu placed in the Xaa position is the most stable conformation for negatively charged residues, it results in a significant decrease in helix stability as exhibited by the RPN value and T_m.

After assembly as described above, transmission electron microscopy (TEM) was employed to interrogate assembled structures after incubation at room temperature for at least one week. In opposition to our original hypothesis that the peptides would form 2D peptide sheets, 1D tubular structures were observed instead. No evidence of ordered assembly was observed upon imaging single peptide solutions, which suggests that assembly of the peptides is dependent the presence of both in solution (Supplemental Figure 11). The macroporous collagen tubes displayed highly polydisperse characteristics including variation in length along the long axis as well as diameter and wall thickness. Figure 9 displays representative tubes of varying structural dimensions.

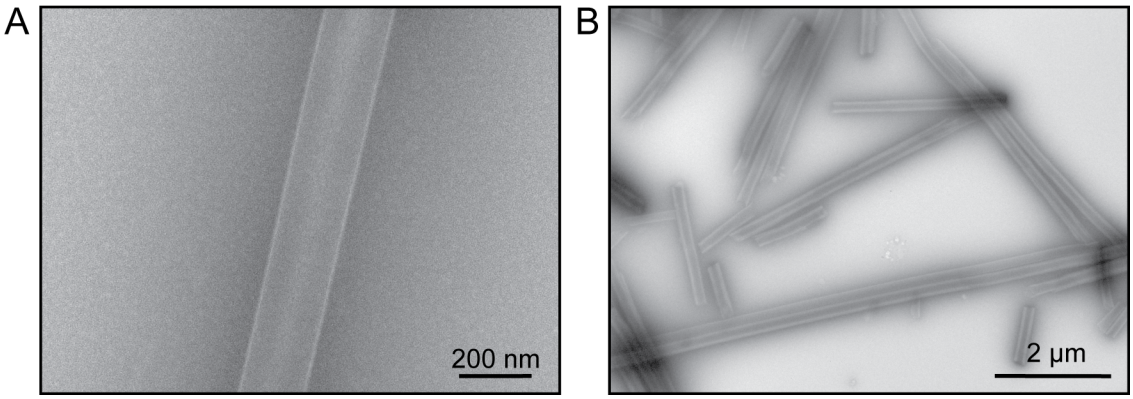

Figure 9. (A) TEM image of a single representative collagen tube constructed from **R4P6** and **P6E4**. (B) TEM image of a polydisperse group of collagen structures.

Assembly size distributions were made through assessing the dimensions of many (N = 56) structures, which were found to be 107.1 ± 30.8 nm in inner diameter and 195.5 ± 19.6 nm in outer diameter. The difference between the diameters represents the tube wall thickness. At

higher magnifications, it becomes possible to visualize distinct layers within the tube walls. An important discovery in constructing a model for the assembly of the tubes was that the thickness of a single lamellar structure is 11.4 ± 1.1 nm. This value roughly corresponds with the expected height for a sheet comprised of peptides 30 residues in length based off the proposed assembly model for a multicomponent peptide sheet (Figure 7). The theoretical height of a collagen triple helix, which represents the height of a sheet where helices pack laterally, is calculated to be 0.286 nm per residue, or 8.58 nm for a 30-residue peptide.[27] Differences between the calculated height of the triple helix and measured wall thickness can be partially rationalized on the basis that the peptide tubes may be distorted while subject to the high vacuum employed for TEM.

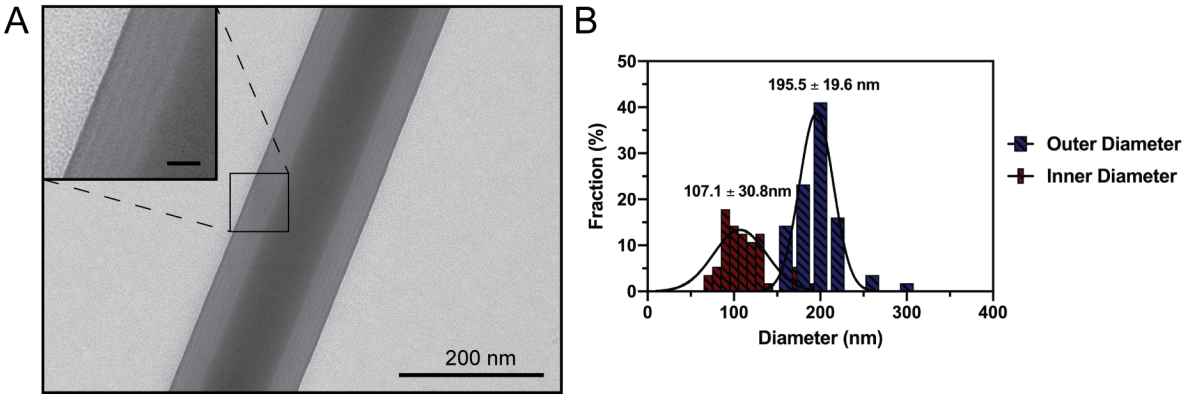

Figure 10. (A) Enlarged image of a **R4P6/P6E4** tube for visualization of distinct layering. Inset scale bar is equal to 20 nm. (B) Histogram of outer diameter (blue) and inner diameter (red) for **R4P6/P6E4** tubes. A Gaussian distribution was fitted to each of the histograms with the average and standard deviation displayed above plot (N = 56).

Atomic force microscopy (AFM) was employed to assess the height of assembled structures. AFM analysis determined that the average height for **R4P6/P6E4** structures was 159 ± 17 nm (N = 3).

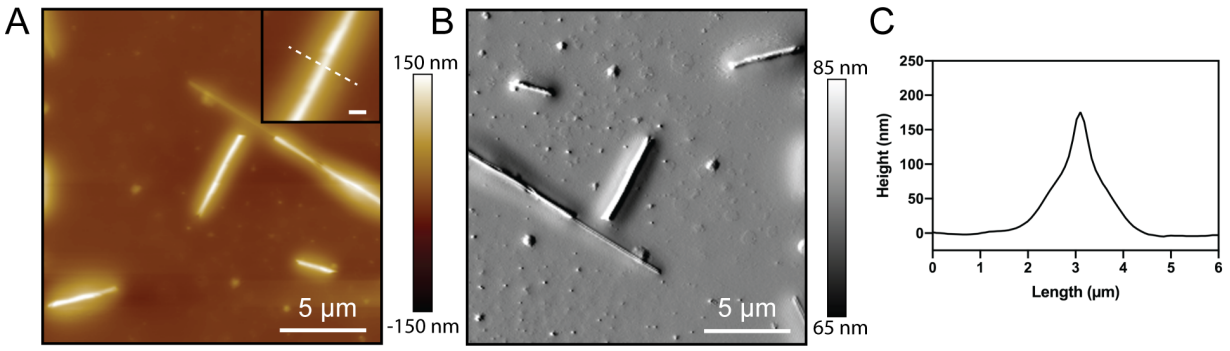

Figure 11. (A) AFM tapping mode topography image of **R4P6/P6E4** peptide tubes. Inset scale bar is equal to 500 nm. (B) AFM tapping mode amplitude image. (C) Line trace depicting the height of the tube indicated in the inset of (A).

AFM measurements are consistent with the formation of macroporous tubes on the scale of over 100 nm in diameter. These results in conjunction with results from TEM are complementary in providing evidence for the structural morphology of the assemblies.

At this point, we introduce an adjustment to the proposed model of assembly represented in Figure 7C. This model, based on published SAXS and electron diffraction of the peptide, **NSI**, shows that previous CMPs assemble into 2D nanoscale peptide sheets through packing into a tetragonal lattice via an antiparallel fashion. The initial proposed assembly model for multicomponent peptide sheets closely resembled the single peptide model in that complementary charge interactions between two peptides with only one type of charge assemble into a tetragonal lattice with antiparallel orientation. However, this model proved to be at least partially limited if not completely invalid because 1D tubular structures were observed rather than 2D nanosheets. We propose that placing charged residues at only a single terminus (*i.e.* asymmetric distribution of charged groups) resulted in a distortion to the assembly where

adjacent helices no longer packed parallel to one another resulting in a 2D sheet that curves into a 1D tubular with many layers.

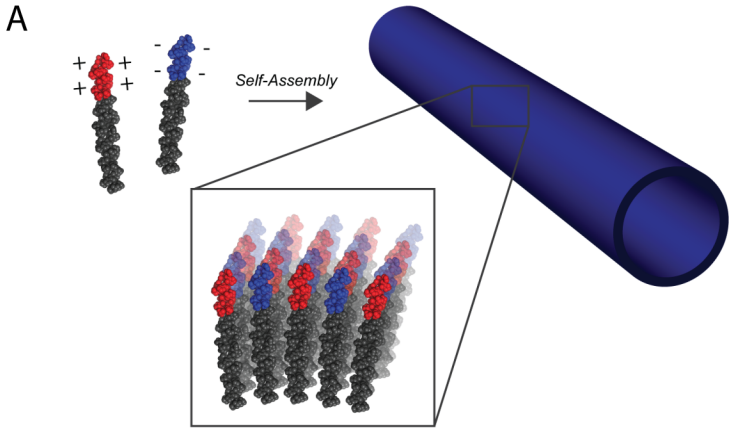

Figure 12. (A) Modified assembly schematic for the formation of multicomponent 1D macroporous tubes.

To further understand the novel structural morphology of collagen exhibited by the peptide tubes, a new peptide sequence was designed. We proposed that this new sequence would assemble into single component 2D peptide nanosheets as a consequence of its symmetric design. The sequence, termed **CP 262** (Figure 13A)**,** contains an identical number of triads and charged blocks as **R4P6** and **P6E4**. Rather than placing all charged triads at a single terminus, two charged triads comprising Glu and Arg were placed at the C and N-terminus (*ie*. symmetric peptide), respectively.

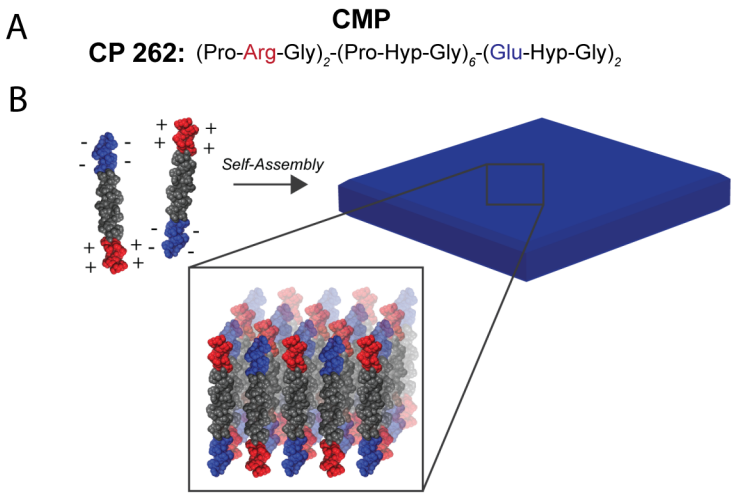

Figure 13. (A) Peptide sequence for **CP 262**. (B) Proposed assembly schematic for **CP 262** 2D peptide nanosheets.

CP 262 was designed as a control experiment to investigate whether the peptide length or total charge constitution resulted in the formation of tubes rather than the asymmetric charge distribution of **R4P6** and **P6E4**.

Initial characterization of **CP 262** included assessment of the triple helical conformation in aqueous buffered solution after annealing. The CD spectrum of **CP 262** in solution displayed characteristic triple helix conformation. An RPN value was calculated to be 0.48 indicating the formation of a stable triple helix. T_m was estimated to be 55 ºC from the minimum of the first derivative of the melting curve, which is considerably higher than **R4P6** and **P6E4**. **CP 262** likely exhibits a significant increase in propensity for forming a triple helix as a result of fewer repulsive charged interactions at the termini.

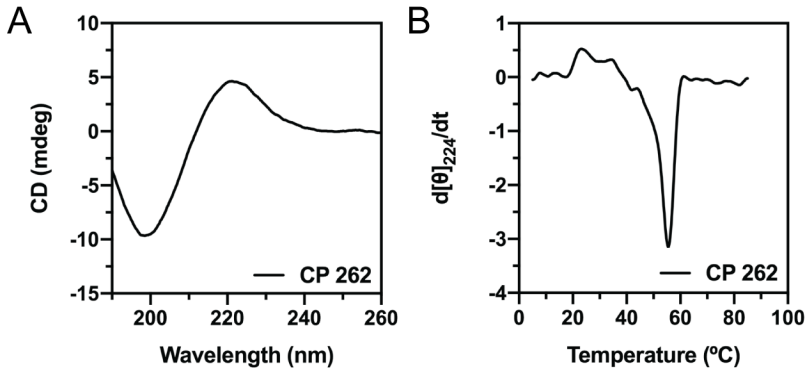

Figure 14. (A) CD spectrum of peptide **CP 262** (1 mg/mL) in 20 mM TAPS buffer, pH 8. (B) First derivative plot of CD signal at 224 nm as a function of increasing temperature for **CP 262** (0.5 mg/mL) in 20 mM TAPS, pH 8.

As predicted, **CP 262** formed large 2D peptide sheets (Figure 15). The nanosheets were polymorphic, spanning a range of sizes on the order of micrometers.

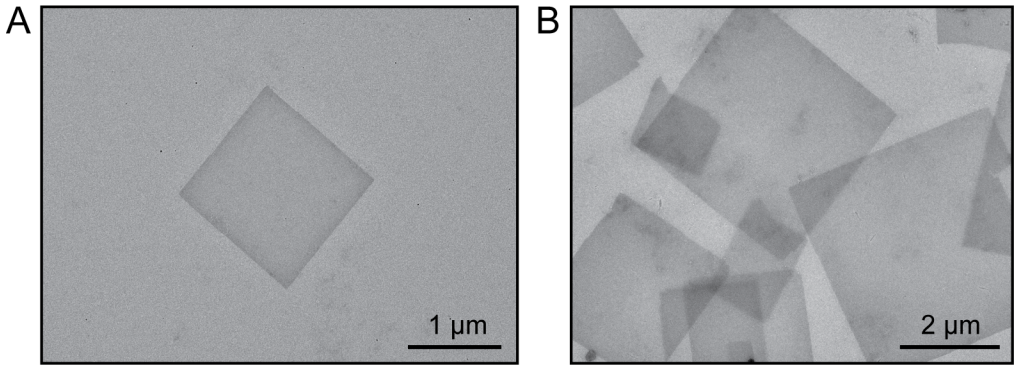

Figure 15. (A) Single representative **CP 262** 2D peptide nanosheet. (B) Many polydisperse **CP 262** 2D peptide nanosheets.

In pursuit of producing a structurally homogeneous population of macroporous collagen tubes with identical diameter and wall thickness, we introduced a modification to the sequence of **R4P6** to include two additional positively charged triads at the N-terminus, terming the new

sequence, **R6P6** (*ie*. increased *m=4* to *m=6* based on Figure 7A). The new peptide sequence, **R6P6**, was designed to have extra positively charged triads protruding from the surface of the peptide tubes with the intention of serving two purposes: firstly, the extra charged triads would prevent the addition of layers to the structures, and secondly, the additional charged triads would create a positive surface charge on the 1D structures thereby preventing non-specific aggregation. A similar sequence modification had been used successfully to create charged collagen nanosheets for the purpose of controlling the formation of layered structures.[24]

As with the initial collagen peptides, **R6P6** was examined first through CD spectropolarimetry at various pH conditions (pH 6, 7, and 8). **R6P6** demonstrated similar stability to **R4P6** with the formation of a stable triple helix at an RPN value of 0.08. **R6P6** displayed a slightly higher T_m (pH 7) at 46ºC, which is attributable to the two additional charged triads at the N-terminus.

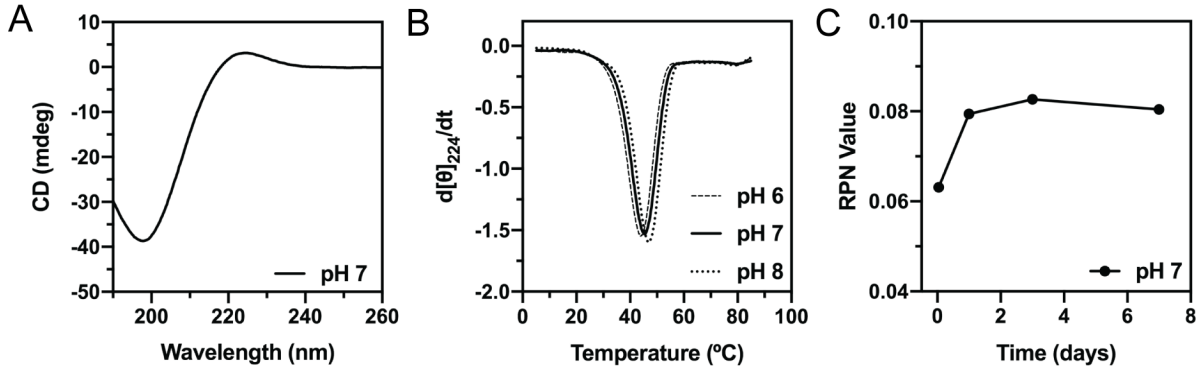

Figure 16. (A) CD spectrum of peptide **R6P6** (1 mg/mL) in 20 mM MOPS buffer, pH 7. (B) First derivative plot of CD signal at 224 nm as a function of increasing temperature for **R6P6** (0.5 mg/mL) in 20 mM MES pH 6, MOPS pH 7, and TAPS pH 8. (C) RPN values at the time points of 1 hour, 24 hours, 3 days and 7 days.

Assembly experiments utilizing **P6E4** as the complementary negatively charged peptide were conducted over a range of pH conditions. Results indicate that at pH 6 and 7, **R6P6** assembled with **P6E4** into large polydisperse irregularly shaped 2D nanosheets. While at pH 8, **R6P6** was observed to assemble into well-defined macroporous tubes larger than those formed using **R4P6**.

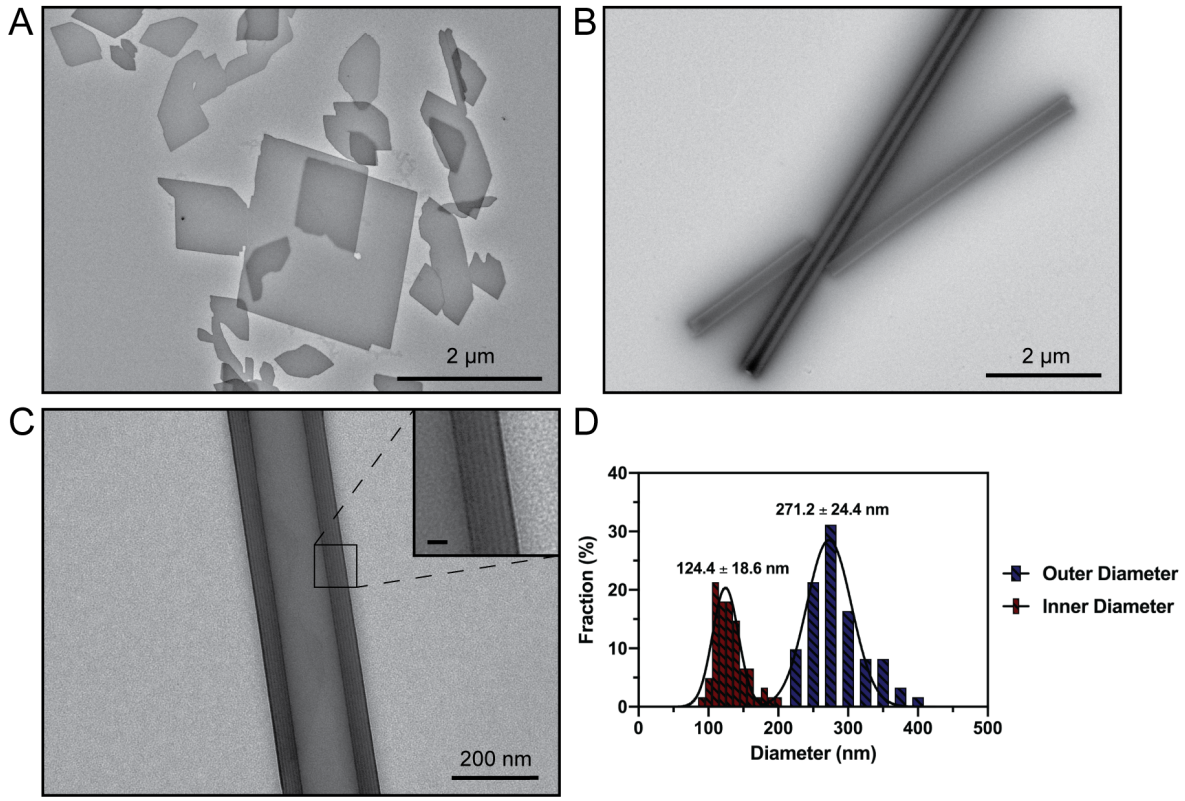

Figure 17. (A) 2D large **R6P6/P6E4** peptide sheets formed at pH 7 (similar to pH 6 structures). (B) Low magnification image of pH 8 **R6P6/P6E4** peptide tubes and (C) higher magnification image of a **R4P6/P6E4** tube for visualization of distinct layering. Inset scale bar is equal to 20 nm. (D) Histogram of outer diameter (blue) and inner diameter (red) for **R6P6/P6E4** tubes. A Gaussian distribution was fitted to each of the histograms with the average and standard deviation displayed above plot (N = 61).

However, despite the formation of peptide sheets at neutral and slightly acidic pH, **R6P6** was observed to form large macroporous collagen tubes at pH 8 similar to those observed initially with **R4P6**. As predicted, the structures exhibited little or no propensity towards nonspecific aggregation, but the additional charged blocks did not prevent the addition of layers to the tube structure. On the contrary, the **R6P6** tubes were observed to contain a higher level of layering with an average of ~6 layers compared to an average of ~3 layers for the **R4P6** derived tubes. The inner diameter of the **R6P6/P6E4** peptide tubes was found to be 124.4 $\pm$ 18.6 nm with an outer diameter of 271.2 $\pm$ 24.4 nm. The average width of each layer was 11.9 $\pm$ 4.6 nm, which is similar to the theoretical height of 10.3 nm for a CMP containing 36 residues.

AFM was employed in order to determine the heights of the 1D and 2D structures assembled. Consistent with prior AFM height measurements of collagen based 2D materials, the height of **R6P6** a pH 7 peptide sheet was 11.3 $\pm$ 1.4 nm averaged across the width of the sheet as depicted in Figure 18D. This value is slightly greater than the theoretical height for the taller of the two peptides, **R6P6**, but is reasonably consistent with the formation of single layer peptide sheets. The average height of the tubes measured was 178 $\pm$ 31 nm (N = 9), which is consistent with the formation of macroporous tubular assemblies. AFM and TEM demonstrate the structural morphology of single layer multicomponent peptide sheets and macroporous tubes.

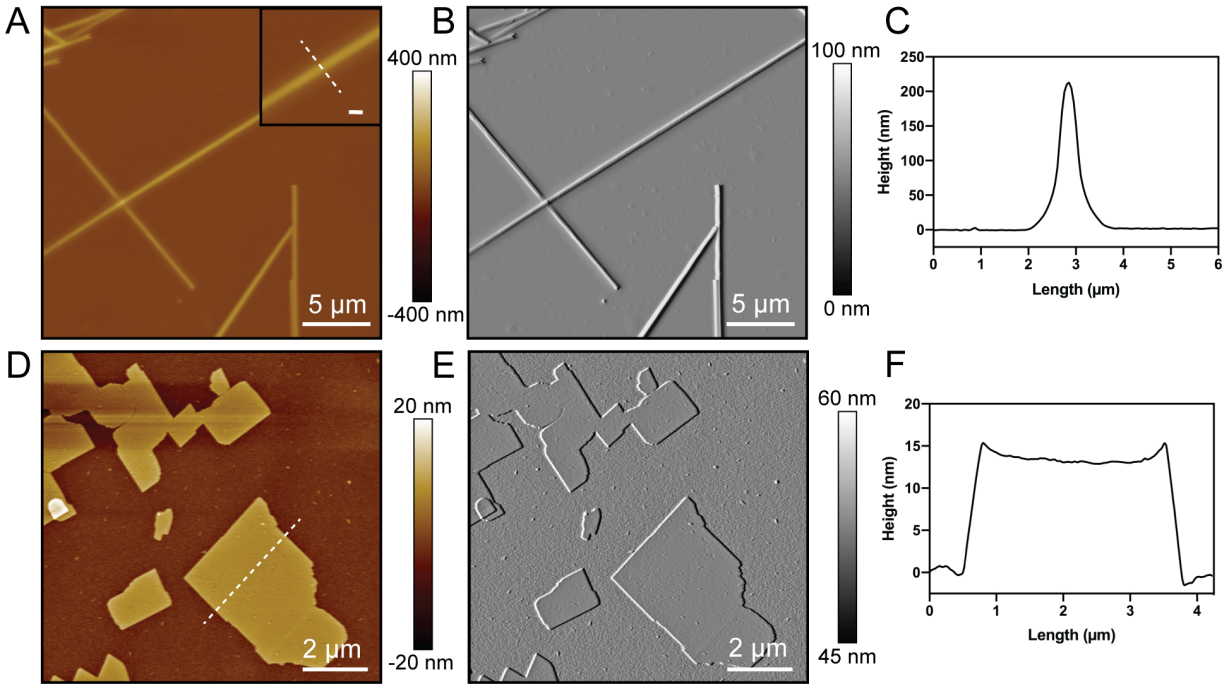

Figure 18. (A) AFM tapping mode topography image of **R6P6/P6E4** peptide tubes. Inset scale bar is equal to 500 nm. (B) AFM tapping mode amplitude image. (C) Line trace depicting the height of the tube indicated in the inset of (A). (D) AFM tapping mode topography image of **R6P6/P6E4** peptide sheets. (E) AFM tapping mode amplitude image. (F) Line trace depicting the height of the sheet across the dashed line in (A).

While continuing to work towards developing a structurally homogeneous population of macroporous single layer peptide tubes, a new approach was designed where we began mixing **R4P6** and **R6P6** into the assemblies with each other. These so-called "doping" experiments incorporated a series of ratios of the two peptides. We found that the doped experiments ranged from forming entirely sheets with more **R6P6** to entirely tubes with more **R4P6**. Furthermore, we observed that the ratios 50%/50% and 75%/25% of **R4P6/R6P6** assembled into only single layer tubes with some interspersed sheets. Analysis of the tri-peptide single layer collagen tubes from TEM indicates the creation of a more monodisperse population of structures than was

found using either peptide on its own. We propose that the doped in **R6P6** incorporates itself randomly into the structure resulting in the tubes inability to form stable layered packing of the triple helices. Investigating this hypothesis would require further structural characterization.

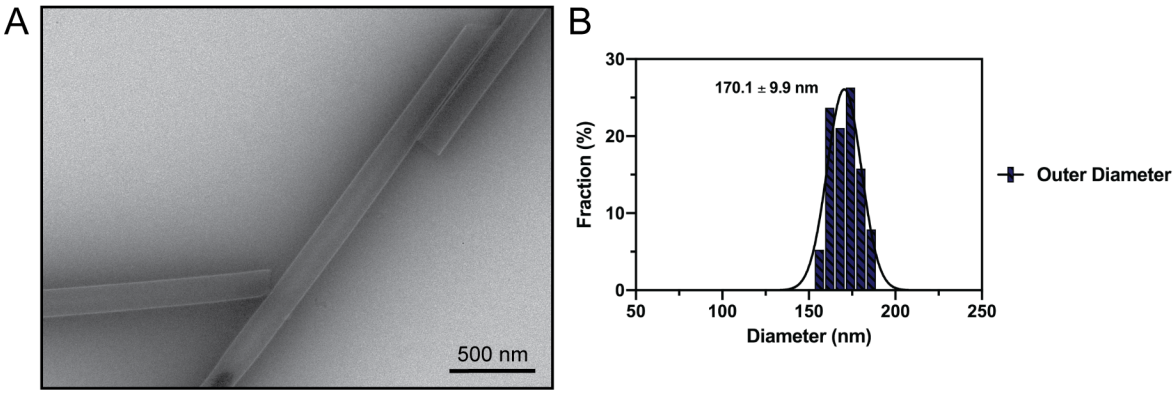

Figure 19. (A) TEM image of doped (50% **R4P6** /50% **R6P6)/P6E4** single walled tubes. (B) Histogram of outer diameter (blue) of doped (50% **R4P6** /50% **R6P6)/P6E4** single walled tubes. A Gaussian distribution was fitted to the histogram with the average and standard deviation displayed above plot.

Introduction of the **R6P6** peptide to the system allowed for two significant developments: first, **R6P6** self-assembles into structures that are more well-defined than those assembled from **R4P6**, and second, the incorporation of **R6P6** allows for a pH mediated transition between 1D and 2D assemblies. Based on these preliminary experiments, we reason that the extra charged triads contribute to creating positive surface charge, which, in turn, results in improved propensity for self-assembly; however, further experiments are needed to fully understand the process. In order to study the surface charge of the assemblies, zeta potential measurements for peptide solutions including multilamellar tubes, single walled tubes, and 2D sheets were conducted. If the proposed assembly model was supported, we would expect the zeta potential,

as a representation of the surface charge, to increase becoming more positive as the relative amount of **R6P6** peptide increased in the assemblies.

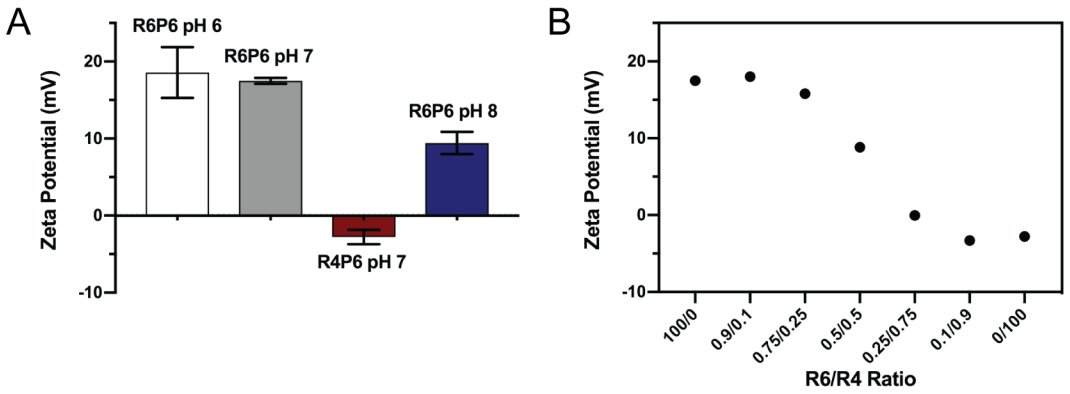

Figure 20. (A) Zeta potential measurements of aqueous buffered solutions of **R6P6** peptide nanosheets at pH 6 (MES, 20mM) and pH 7 (MOPS, 20 mM) as well as peptide tubes comprising **R4P6** (MOPS pH 7, 20mM) or **R6P6** (TAPS pH 8, 20mM). (B) Zeta potential dependence on the relative concentrations of **R6P6** and **R4P6** for doped tri-peptide assembly experiments all performed in pH 7 buffer (MOPS, 20mM).

In support of our hypothesis, the data demonstrates that the **R6P6** peptide sheets at pH 6 had the most positive zeta potential *ca*. +18 mV while the **R4P6** peptide tubes at pH 7 displayed the most negative zeta potential of *ca*. -3 mV. Furthermore, for mixtures of **R4P6/R6P6**, a gradient of decreasing zeta potential was observed as the ratio of **R6P6/R4P6** decreased. The zeta potential measurements support the proposed model where extra positive triads create positive surface charge for the assemblies in solution, but does not help rationalize the continued observation of multilamellar tubes as seen with **R6P6** assemblies at pH 8. The observation of macroporous tubes at pH 8 compared to 2D peptide nanosheets at pH 7 and 6 with identical peptide content demonstrates that surface charge may be a key mediator in the final assembly morphology.

In an attempt to correlate the surface charge observed through zeta potential with the topology of the nanosheets and tubes, a series of experiments were conducted with cationic (15 nm amine functional) and anionic (15 nm carboxylate functional) gold nanoparticles. We hypothesized that the anionic gold nanoparticles would selectively adsorb onto the positively charged surfaces of the peptide sheets and tubes, while the cationic particles would experience unfavorable repulsion from the structures and would therefore not adsorb onto the surfaces.

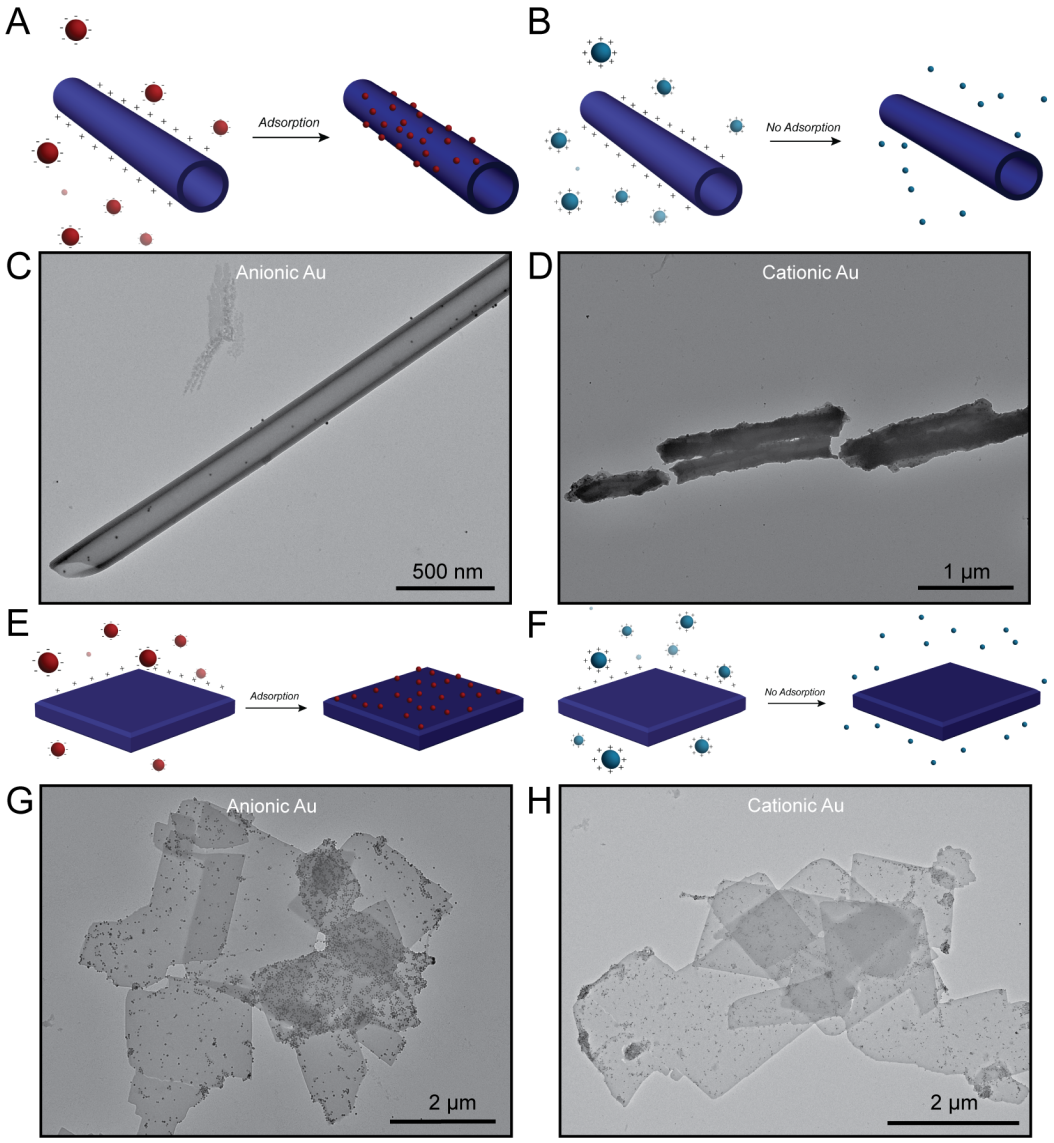

Figure 21. (A) Proposed interaction between anionic Au particles and (B) cationic Au particles with the peptide tubes. (C) TEM of anionic Au particle and (D) cationic particle interactions with

the peptide tubes. (E) Proposed interaction between anionic Au particles and (F) cationic Au particles with the peptide nanosheets. (G) TEM of anionic Au particle and (H) cationic particle interactions with the peptide nanosheets.

Contrary to our hypothesis, we observed that both types of gold nanoparticles displayed an affinity for the peptide structures, and, at higher concentration, the gold particles were found to degrade the structures significantly. It seems likely that the charge distributions on the particles interfered with the electrostatic interactions holding the assembled structures together resulting in degradation. Despite results contraindicating our hypothesis, we can rationalize our observation in part based on the proposed assembly model. The assembly model suggests that the sheets and tubes will have one surface that is positively charged while the other is relatively neutral. It is conceivable that the negative particles interact with the positive face as predicted, but, in contrary to our prediction, it is also possible that the positive particles could interact with exposed negative charges on the neutral face of the structures.

While zeta potential and gold nanoparticle experiments do not prove that the surface charge is associated with the topography, they do partially support the hypothesis that **R6P6** is incorporated into the assembled sheets. However, these results disagree with the proposed hypothesis that positively charged surfaces would result in the inability for the peptides to form multilamellar tubes. **R6P6** displayed an even higher propensity for layering with a higher average number of layers. To rationalize this result, we propose that the packing of the triple helices in the **R6P6** tubes changes as a result of a higher pH with less positive surface charge as demonstrated through a more neutral zeta potential of *ca*. +8 mV. The possible alteration in packing may allow multilayer tubes to form regardless of the two additional charged triads and

perhaps creates a more ordered structure resulting in larger tubes with additional layers. This hypothesis can be further evaluated through diffraction experiments such as small angle X-ray scattering (SAXS).

Knowing that **R6P6** assembles into defined 2D structures at pH 6 and 1D structures at pH 8, we proposed that one can control the interconversion between the two structures via pH changes of the assembly medium. Using HCl and NaOH, titration experiments were performed where sheets at pH 6 were titrated to pH 8 and *vice versa*. As predicted, after one week of incubation the structures had transitioned to reflect the preferred assembly morphology for the final pH condition. Despite the interconversion, the mechanism of transition remains unknown. We propose that the transition is possibly a disassembly followed by a reassembly into the alternate morphology or that the structures remain intact and transition through either a rolling or unrolling motion. Up to this point there is no definitive evidence on the mechanism of transition. The experiment demonstrates the successful pH-controlled mediation between two multicomponent peptide assemblies.

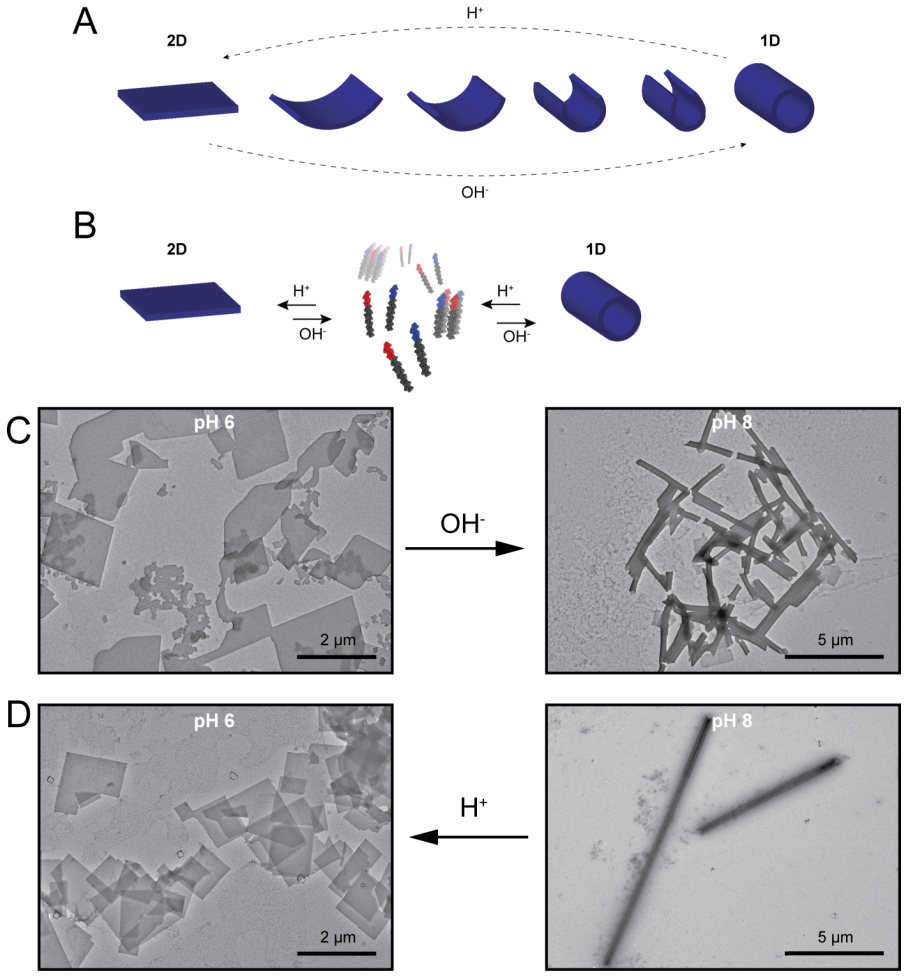

Figure 22. (A) Proposed transition mechanism without and (B) with disassembly. (C) pH 6 structures titrated to pH 8 and (D) pH 8 structures titrated to pH 6 transforming from sheets to tubes and vice versa.

Prior work with collagen nanostructures has demonstrated that utilization of the biotin-streptavidin interaction allows for the functionalization of CMP based peptide materials. A biotin-conjugated **R6P6** peptide was synthesized using a D-biotin-15-amido-4,7,10,13-dioxapentadecyl group (biotin-PEG2-acid) that was selectively placed at the N-terminus connected through a $(PEG)_2$ linker. The biotinylated peptide was incorporated into the **R6P6** annealing process forming heteromeric triple helices and assembled into sheets and tubes at pH 7

and 8, respectively. The structures appeared indistinguishable from those containing only **R6P6**, as shown above in Figure 17A-B (Supporting Figure 12). The structures were mixed with Cy3B tagged streptavidin and imaged using stochastic optical reconstruction microscopy (STORM). Fluorescent structures were observed for both assemblies as depicted in Figure 23.

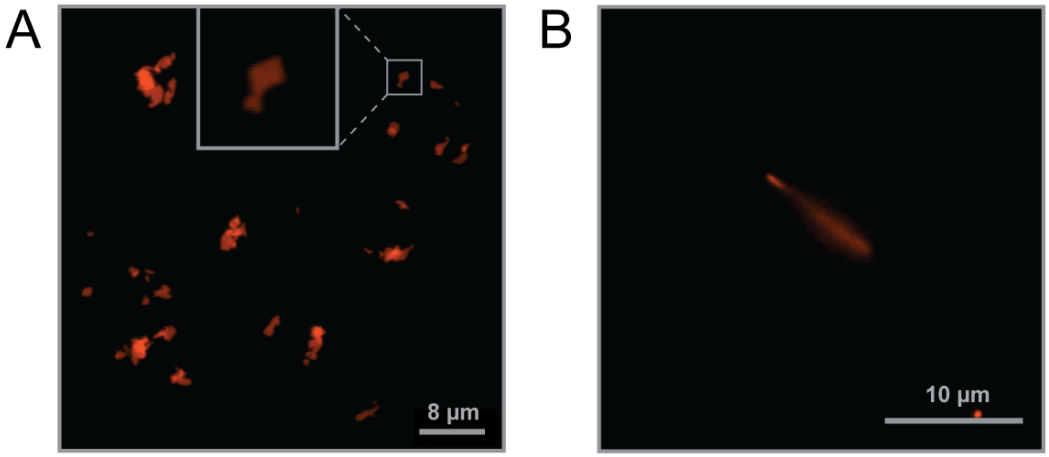

Figure 23. (A) Fluorescent microscopy image of pH 7 **R6P6/P6E4** 2D peptide nanosheets functionalized with biotin-streptavidin conjugated to Cy3B dye. (B) Fluorescent microscopy image of pH 8 **R6P6/P6E4** 1D peptide tube functionalized with biotin-streptavidin conjugated to Cy3B dye.

The use of biotin-streptavidin to tag the structures with a fluorophore serves as a proof of concept that the structures assembled and characterized in this thesis can be functionalized with a high degree of specificity.

Conclusion

We demonstrate that the assembly space for CMPs can be expanded through the use of incorporating multiple complementary peptides into assembled structures. Furthermore, the development of multicomponent peptide systems has a higher degree of functionality, but more

significantly, serves as a bridge between 1D and 2D peptide materials in a manner that has not been previously described. The described peptide macroporous tubes are larger than any of those previously reported in the literature, as far as we are aware, as well as being the first of such reported structures made from CMPs. The 2D multicomponent peptide sheets developed are an improvement on similar structures reported thus far in the literature resulting most probably from using an antiparallel design rather than a parallel design. Initial results indicate that the structures can be successfully functionalized through the use of biotin-streptavidin interaction and have the potential for a range of uses including vessels for the encapsulation of larger molecules, templates for the construction of more complex devices organized through a bottom-up fashion, sensing and structural supports for higher order assembly, to name a few.

Despite the progress reported in this thesis, much remains to investigate. Many assertions about the structure of the materials assembled were made based on a proposed assembly model without any further verification. We believe that the proposed assembly model has merit, but to further understand the structures additional methods of characterization are necessary. Such methods that could be employed to interrogate the packing of the collagen helices are SAXS, powder diffraction, and cryo-EM. Based on the structural data of previously characterized structures, it may also be possible to develop a computationally derived model for the reported multicomponent materials. Through furthering our knowledge of the structures created, we can better develop and implement design principles for future projects with specific aim to developing mesoscale structural control over the assemblies as well as the fine-tuning of their properties, which both address current limitations in the field of materials science.

Other future directions for this project pertain to their possible future utility across a variety of functionalities. Data presented in this thesis demonstrates proof of concept that the

tubes can be functionalized through biotin-streptavidin interaction via binding of a Cy3B-streptavidin fluorophore to the **R6P6** component of the assemblies. These results demonstrate one possible functionality of the structures, but in principle, the structures have the ability to be functionalized in a variety of ways including biorthogonal functionalization. While utilization of multiple functional groups to decorate the assemblies with small molecules is a novel demonstration for collagen based macroporous tubes, we also aim to use the functional sites to bind larger molecules such as enzymes for catalysis or antibodies for selective binding of antigens. In conclusion, the mesoscale tubular structures reported in this thesis possess a high degree of potential for future application through their increased potential for functionality as well as their mechanical properties.

CMPs have been demonstrated to be highly versatile in their incorporation into nanoscale and larger structures. Moreover, the collagen triple helix, through formation into a rigid rod-like building block, represents a highly tactile unit from which to construct more complex hierarchical structures. Current research aspires to continue to improve the structural definition from nanoscale to mesoscale order for future utility in nanotechnology, molecular biology, and other fields.

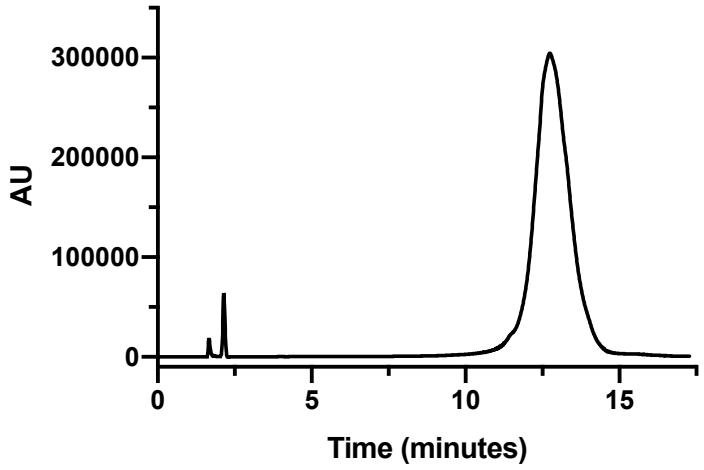

Figure S1. HPLC trace for **R4P6**.

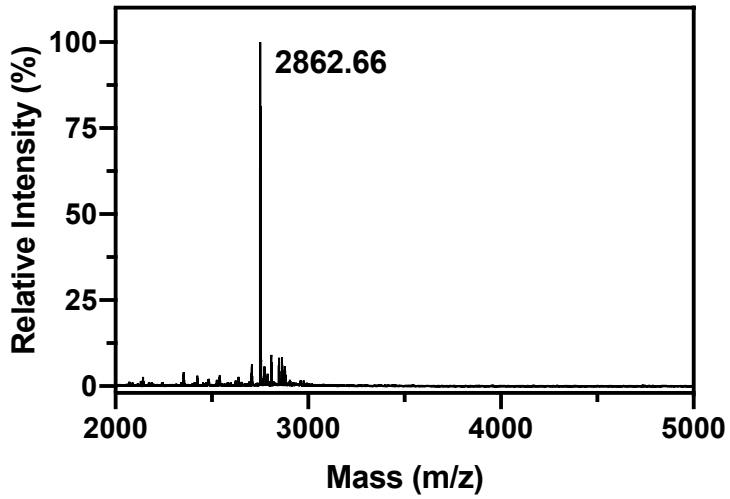

Figure S2. MALDI-TOF mass spectrum of the peptide, **R4P6,** after HPLC re-purification.

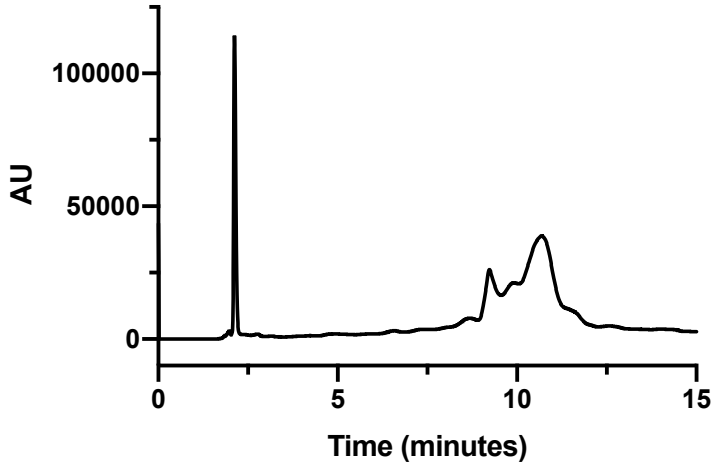

Figure S3. HPLC trace for **P6E4**.

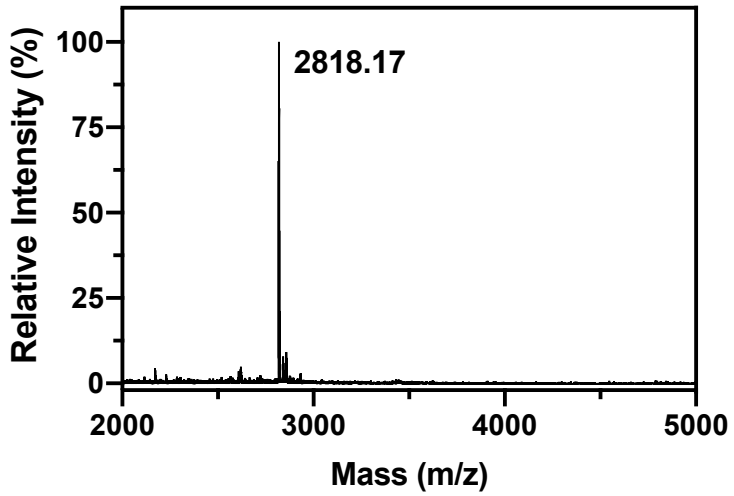

Figure S4. MALDI-TOF mass spectrum of **P6E4** after HPLC re-purification.

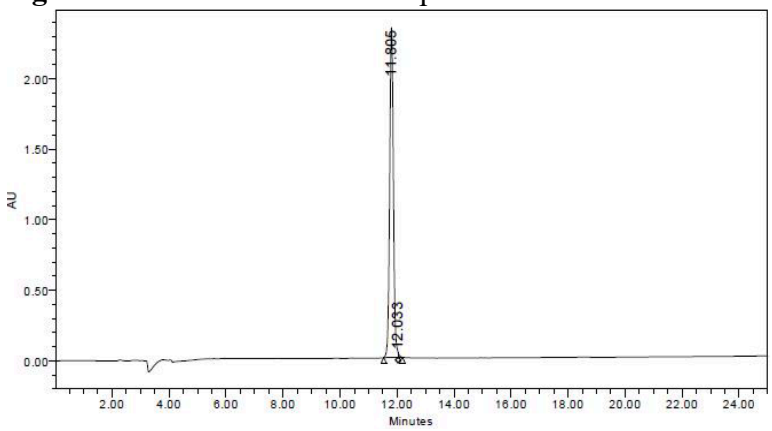

Figure S5. HPLC trace for **R6P6** (SynPep).

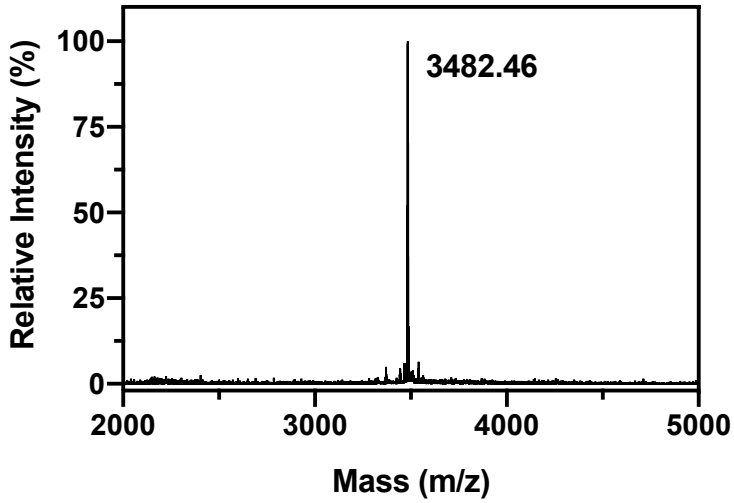

Figure S6. MALDI-TOF mass spectrum of **R6P6** after dialysis.

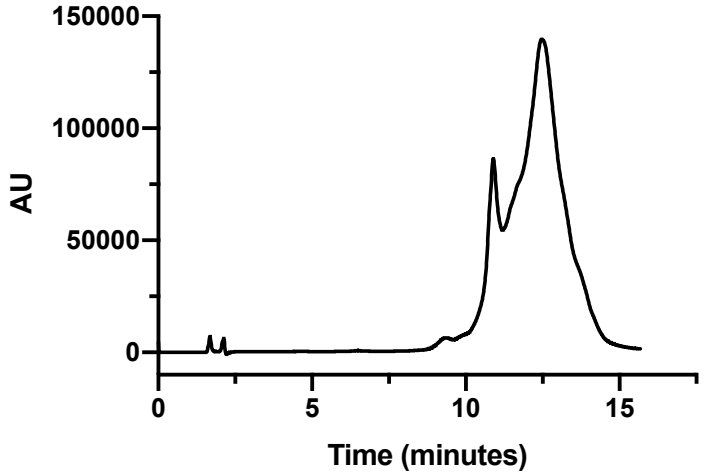

Figure S7. HPLC trace for **CP 262**.

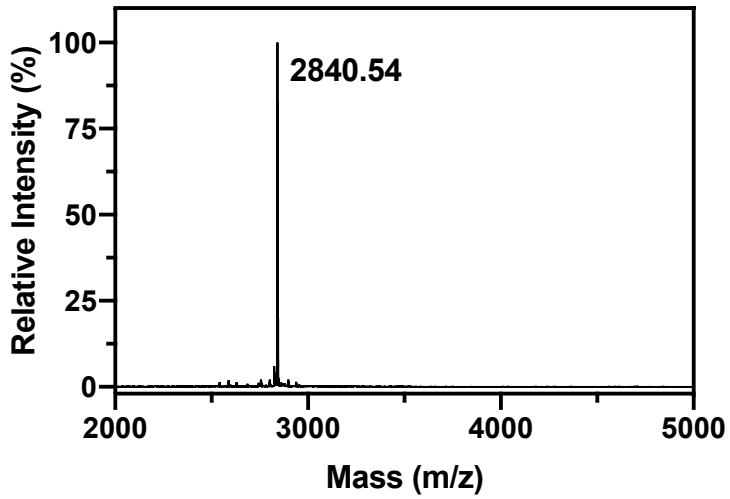

Figure S8. MALDI-TOF mass spectrum of **CP 262** after HPLC re-purification.

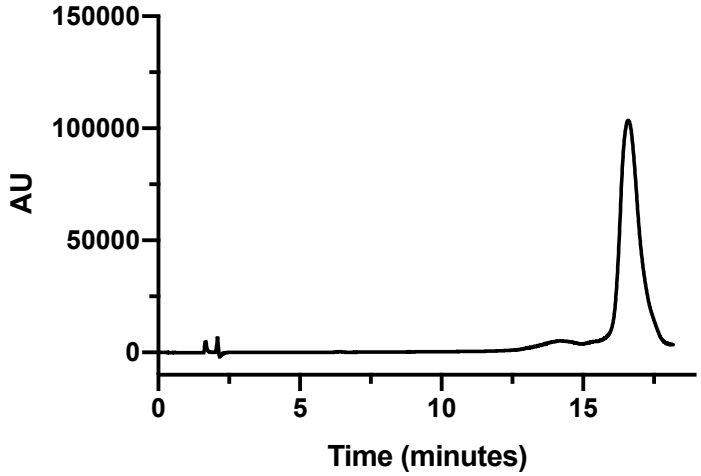

Figure S9. HPLC trace of **Biotin-R6P6**.

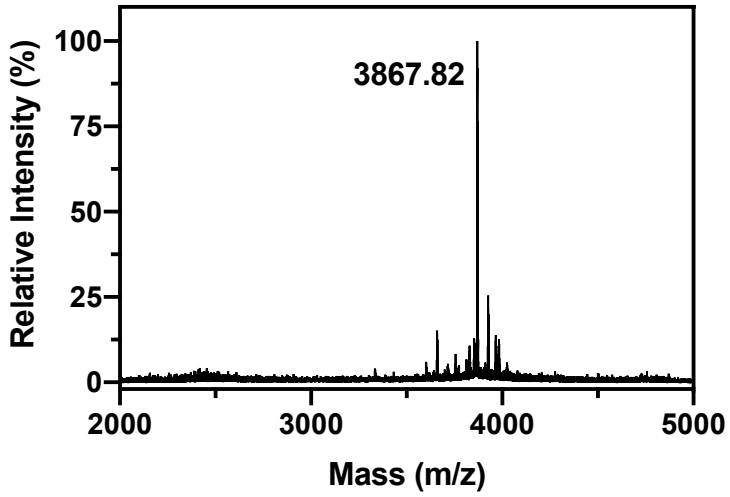

Figure S10. MALDI-TOF mass spectrum of **Biotin-R6P6** after HPLC re-purification.

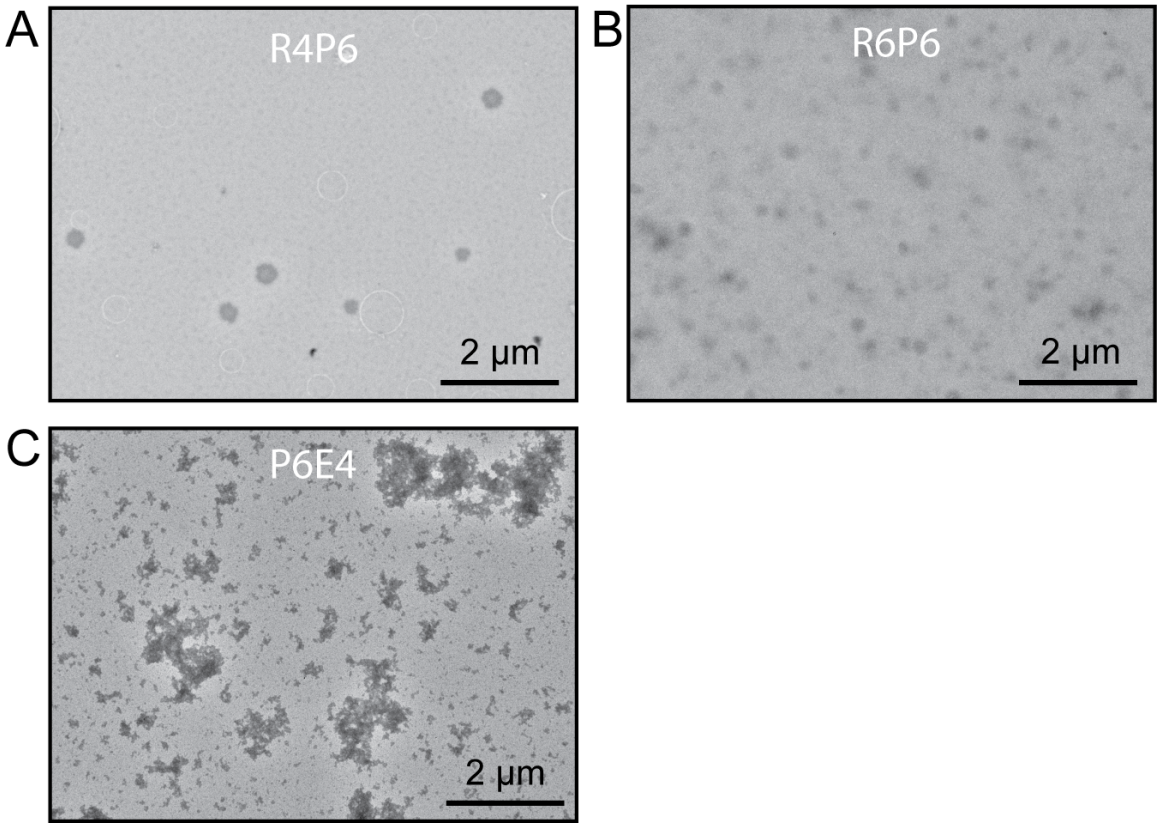

Figure S11. (A) Control TEM of individual peptide **R4P6**, (B) **R6P6**, and (C) **P6E4**.

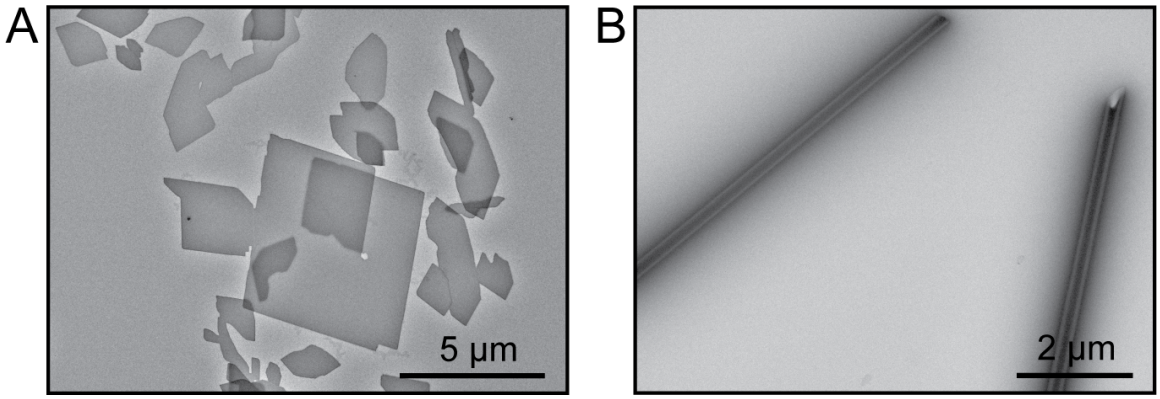

Figure 12. (A) **Biotin-R6P6/P6E4** pH 7 peptide nanosheets and (B) **Biotin-R6P6/P6E4** pH 8 peptide tubes.

References

[1] Boott, C. E.; Nazemi, A. and Manners, I. Synthetic Covalent and Non-Covalent 2D Materials. *Angewandte Chemie* **2015**. *54*, 13876-13894.

[2] Giorno L., Piacentini E., Bazzarelli F. (2015) Macroporous, Mesoporous, and Microporous Membranes. In: Drioli E., Giorno L. (eds) Encyclopedia of Membranes. Springer, Berlin, Heidelberg.

[3] Tian, Y.; Polzer, F. B.; Zhang, H. V.; Kiick, K.; Saven, J. G. and Pochan, D. J. Nanotubes, Plates, and Needles: Pathway-Dependent Self-Assembly of Computationally Designed Peptides. *Biomacromolecules.* **2018.** *19,*4286-4298.

[4] Sirohi, D.; Chen, Z.; Sun, L.; Klose, T.; Pierson, T. C.; Rossmann, M. G. and Kuhn, R. J. The 3.8 Å resolution cryo-EM structure of Zika virus. *Science*. **2016**. *352 (3284)*, 467-740.

[5] Grotjahn, D. A.; Chowdhury, S.; Xu, Y.; McKenny, R. J.; Schroer, T. A. and Lander, G. C. Cryo-electron tomography reveals that dynactin recruits a team of dyneins for processive motility. *Nature Structural & Molecular Biology.* **2018**. *25*, 203-207.

[6] Letts, J. A. and Sazanov, L. A. Clarifying the supercomplex: the higher-order organization of the mitochondrial electron transport chain. *Nature Structural & Molecular Biology.* **2017.** *24*, 800-808.

[7] Gao J.; Wang H.; Yuan Q. and Feng Y. Structure and Function of the Photosystem Supercomplexes. *Front Plant Sci*. **2018**. *9,* 1-7.

[8] Hamley, I. W. Nanotechnology with Soft Materials. *Angewandte Chemie*. **2003**. *42*, 1692-1712.

[9] Ghadiri, M. R.; Granja, J. R.; Milligan, R. A.; McRee, D. E. and Khazanovich. Self-assembling organic nanotubes based on a cyclic peptide architecture. *Nature*. **1993.** *366*, 324-327.

[10] Chen, K. H.; Corro, K. A.; Le, S. P. and Nowick, J. S. X-ray Crystallographic Structure of a Giant Double-Walled Peptide Nanotube Formed by a Macrocyclic β-sheet Containing $A\beta_{16-22}$. *Journal of the American Chemical Society.* **2017**. *139,* 8102-8105.

[11] Webber, M. J.; Appel, E. A.; Meijer, E. W. and Langer, R. Supramolecular biomaterials. *Nature Materials.* **2016**. *15,* 13-26.

[12] Shen, H.; Fallas, J. A.; Lynch, E.; Sheffler, W.; Parry, B.; Jannetty, N.; Decarreau, J.; Wagenbach, M.; Vicente, J. J.; Chen, J.; Wang, L.; Dowling, Q.; Oberdorfer, G.; Stewart, L.; Wordeman, L.; Yoreo, J. D.; Jacobs-Wagner, C.; Kollmann, J. and Baker, D. De novo design of self-assembling helical protein filaments. *Science*. **2018**. *362,* 705-709.

[13] Nam, K. T.; Shelby, S. A.; Choi, P. H.; Marciel, A. B.; Chen, R.; Tan, L.; Chu, T. K.; Mesh, R. A.; Lee, B.; Connolly, M. D.; Kisielowski, C. and Zuckermann, R. N. Free-floating ultrathin two-dimensional crystals from sequence-specific peptoid polymers. *Nature Materials*. **2010**. *9*, 454-460.

[14] He, X.; Hxiao, M.; Boott, C. E.; Harniman, R. L.; Nazemi, A.; Li, X.; Winnik, M. A. and Manners, I. Two-dimensional assemblies from crystallizable homopolymers with charged termini. *Nature Materials*. **2017**. *16*, 481-488.

[15] Qiu, H.; Gao, Y.; Boott, C. E.; Gould, O. E. C.; Harniman, R. L.; Miles, M. J.; Webb, S. E. D.; Winnik, M. A. and Manners, I. Uniform patchy and hollow rectangular platelet micelles from crystallizable polymer blends. *Science*. **2016**. *352 (6286)*, 697-700.

[16] Jin, H.; Ding, Y.; Wang, M.; Song, Y.; Liao, Z.; Newcomb, C. J.; Wu, X.; Tang, X.; Li, Z.; Lin, Y.; Yan, F.; Jian, T.; Mu, P. and Chen, C. Designable and dynamic single-walled stiff

nanotubes assembled from sequence-defined peptoids. *Nature Communications*. **2018**. *9,* 270-281.

[17] Freeman, R.; Han, M.; Álvarez, Z.; Lewis, J. A.; Wester, J. R.; Stephanopoulos, N.; McClendon, M. T.; Lynsky, C.; Godbe, J. M.; Sangji, H.; Luijten, E. and Stupp, S. I. Reversible self-assembly of superstructured networks. *Science.* **2018***. 362*, 808-813.

[18] Lodish H, Berk A, Zipursky SL, et al. Molecular Cell Biology. 4th edition. New York: W. H. Freeman; 2000. Section 22.3, Collagen: The Fibrous Proteins of the Matrix. Available from: https://www.ncbi.nlm.nih.gov/books/NBK21582/

[19] Rele, S.; Song, Y.; Apkarian, R. P.; Qu, Z.; Conticello, V. P. and Chaikof, E. L. D-Periodic Collagen-Mimetic Microfibrils. *Journal of the American Chemical Society*. **2007**. *129,* 14780-14787.

[20] Jiang, T.; Xu, C.; Liu, Y.; Liu, Z.; Wall, J. S.; Zuo, X.; Lian, T.; Saliata, K.; Ni, C.; Pochan, D. and Conticello, V. P. Structurally Defined Nanoscale Sheets from Self-Assembly of Collagen-Mimetic Peptides. *Journal of the American Chemical Society.* **2014**. *136,* 4300-4308.

[21] Jiang, T.; Xu, C.; Zuo, X. and Conticello, V. P. Structurally Homogeneous Nanosheets from Self-Assembly of a Collagen-Mimetic Peptide. *Angewandte Chemie*. **2014**. *53*, 8367-8371.

[22] Jiang, T.; Vail, O. A.; Jiang, Z.; Zuo, X. and Conticello, V. P. Rational Design of Multilayer Collagen Nanosheets with Compositional and Structural Control. *Journal of the American Chemical Society*. **2015**. *137,* 7793-7802.

[23] Okesola, B. O. and Mata, A. Multicomponent self-assembly as a tool to harness new properties from peptides and proteins in material design. **2018**. *47*, 3721-3736.

[24] Jiang, T.; Xu, C.; Liu, Y.; Liu, Z.; Wall, J. S.; Zuo, X.; Lian, T.; Saliata, K.; Ni, C.; Pochan, D. and Conticello, V. P. Structurally Defined Nanoscale Sheets from Self-Assembly of Collagen-Mimetic Peptides. *Journal of the American Chemical Society.* **2014**. *136,* 4300-4308.

[25] Parmar, A. S.; James, J. K.; Grisham, D. R.; Pike, D. H. and Nanda, V. Dissecting Electrostatic Contributions to Folding and Self-Assembly Using Designed Multicomponent Peptide Systems. *Journal of the American Chemical Society.* **2016**. *138,* 4362-4367.

[26] Persikov, A. V.; Ramshaw, J. A. M. and Brodsky, B. Prediction of Collagen Stability from Amino Acid Sequence. *The Journal of Biological Chemistry.* **2005.** *280*, 19343-19349.

[27] Okuyama, K.; Xu, X.; Iguchi, M. and Noguchi, K. Revision of Collagen Molecular Structure. *Biopolymers*. **2005.** *84*, 181-191.